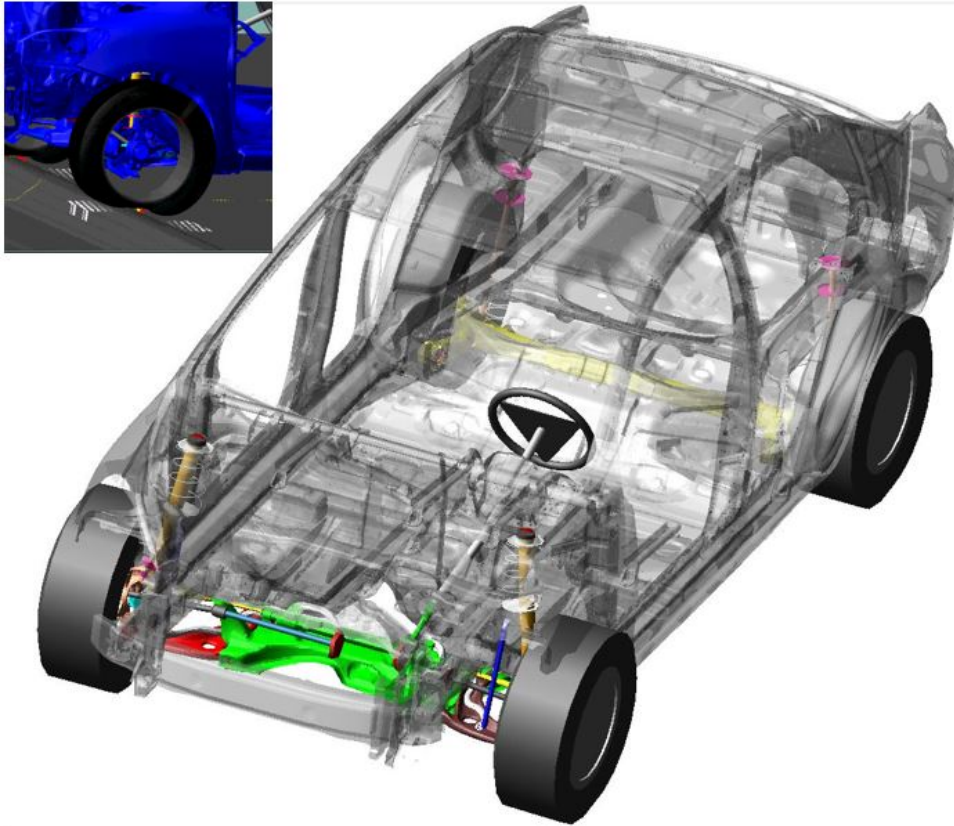




CHALMERS
UNIVERSITY OF TECHNOLOGY



Virtual Full Vehicle Durability Testing of a passenger car

Master's thesis in Automotive Engineering

Darshan Yerandahalli Munirama Reddy
Shankar Padmanabhan

MASTER'S THESIS 2017:84

Virtual Full Vehicle Durability testing of a passenger car

Darshan Yerandahalli Munirama Reddy
Shankar Padmanabhan



Department of Applied Mechanics
Division of Dynamics
CHALMERS UNIVERSITY OF TECHNOLOGY
Gothenburg, Sweden 2017

Virtual Full Vehicle Durability testing of a passenger car
Darshan Yerandahalli Munirama Reddy
Shankar Padmanabhan

© Darshan Yerandahalli Munirama Reddy, Shankar Padmanabhan, 2017.

Supervisors:

Mehdi Mehrgou, AVL List GmbH

Andreas Andblad, AVL MTC Motortestcenter AB

Examiner: *Håkan Johansson*, Division of Dynamics, Chalmers University of Technology

Master's Thesis 2017:84

ISSN:1652-8557

Department of Applied Mechanics

Division of Dynamics

Chalmers University of Technology

SE-412 96, Göteborg

Telephone +46 31 772 1000

Cover: Vehicle Model, Vehicle driving over the curb.

Chalmers Reposervice
Göteborg, Sweden 2017

Virtual Full Vehicle Durability Testing of a Passenger Car
Masters' Thesis in Automotive Engineering
DARSHAN YERANDAHALLI MUNIRAMA REDDY
SHANKAR PADMANABHAN
Department of Applied Mechanics
Chalmers University of Technology

Abstract

In this study, a methodology for full dynamic vehicle durability testing is implemented virtually using the *modal superposition method*. *Stochastic* and *Deterministic* models of roads such as cobblestone, washboard, cleat and rough roads are created based on ISO standards and test data using MATLAB-Simulink and OpenCRG.

Subsequently, a wholly flexible vehicle model of a passenger car is created in ADAMS/Car. Non-linear damper models and bushing models are used as part of the suspension model. Models such as MF-Pacejka 2002 (3D enveloping), FTire are used as the tire models. The elastic characteristics of an FE model is imported into ADAMS/Car by importing the orthogonalized component modes obtained by *Craig-Bampton* reduction of the FE model. The vehicle is simulated on the virtual roads in ADAMS/Car and the modal coordinates of the front suspension LCA are obtained. Therefore, the resulting stress distribution on the LCA is obtained by combining the *modal coordinates* obtained from the dynamic MBS simulations with the stress data of the orthogonalized component modes from the FE analysis in the software FEMFAT.

The effect of different tire models on the stress distribution of LCA when simulated on the roads such as pothole, rough road and curb are investigated. Additionally, the effect of the presence and absence of windshields and masses on the natural frequencies and mode shapes of the body-in-white are investigated.

Some of the key findings of this work are:

- A comparison is made between the developed roads and the actual roads by comparing their PSD spectrum. It is found that they highly correlate. The *damage index* [21] from a vehicle test for a specific component could be used to approximate the road tested to develop a simulated road model.
- The *FTire* model is highly suited for durability simulations involving high frequency vibrations of the order 200Hz as compared to MF Pacejka 2002 (3D Enveloping) and University of Arizona (UA-Tire) tire models. The Pac2002 model could be used as an alternative if FTire is not available only in the frequency ranges up to 80Hz. Additionally, *RMOD-K* tire model, which is an open source model could be used in place of the FTire model for high frequency vibrations.

-
- It is found that Pac2002 (3D Env) underestimates the stress distribution on the LCA, whereas UA-Tire overestimates the stress. The stress distribution on the LCA when FTire is used is found to correlate with the stress distribution from [5].
 - The total number of modes of the BiW reduces as the masses and windshields are added. Also, as the masses are added, the natural frequency of a given mode number reduces.
 - With the current hardware and software capabilities, it is found that this method of virtual vehicle testing is highly feasible. Intel i7 with 4 cores was used through out this project.

Keywords: Durability testing, Vehicle Dynamics, NVH, Modal stress recovery, full vehicle testing, virtual roads, multibody, Gaussian, Laplace moving average, modal superposition, Virtual Proving Ground (VPG).

**கற்க கசடறக் கற்பவை கற்றபின்
நிற்க அதற்குத் தக.**

*(Let a man learn thoroughly whatever he may learn,
and let his conduct be worthy of his learning.)*

-Thiruvalluvar

**It is not knowledge, but the act of learning, not
possession but the act of getting there, which
grants the greatest enjoyment.**

- Carl Friedrich Gauss



A Saab 93 being tested on the track at Trollhättan [1]

Acknowledgements

This thesis was carried out at AVL MTC Motortestcenter AB, Göteborg, Sweden under supervision from AVL List GmbH, Graz, Austria as part of the our degree in *M.Sc Automotive Engineering*.

We are immensely grateful and would like to thank those special people in both AVL Sweden and Austria whose support and contributions meant a lot to us and made this huge project a successful one.

- We would like to thank our supervisor *Mehdi Mehrgou* (AVL List GmbH, Austria) for his immense trust and confidence in us to carry out this project remotely and to facilitate our working from the AVL Sweden. His support, drive and valuable inputs at every step of the project was highly instrumental in making our thesis what it is. And, for inviting us to Graz, Austria and providing us with a enriching learning experience.
- To our supervisor in Sweden *Andreas Andblad* (AVL MTC, Sweden) for providing us with the office space and all the resources that we requested for which made our work easier by many folds. Also, special thanks to him for facilitating our travel to Graz and making our stay at AVL Sweden highly enjoyable.
- To our examiner *Håkan Johansson*, for being our sounding board with whom we could discuss our ideas and for keeping us on the right track.
- To our colleagues at Austria, *Clarissa Holzer* and *Stefan Maier* for being the backbone of our thesis and supporting us with the flexible bodies and FEMFAT, answering our questions and well, for everything. To our colleague *Wakana Sugihara* and her team for patiently providing us with the IT support whenever we asked for. We would also like to thank *Rishikesh Mokashi* and his team at MSC Software for providing us timely support with our questions regarding ADAMS/Car, *Christoph Priestner* (AVL Austria) for assisting us by answering our questions which made all the difference in our results.
- Lastly, but definitely not the least, we would like to thank our parents for their love and unwavering support throughout our Masters’.

Shankar Padmanbhan and Darshan Y.M Reddy,
Göteborg, Sweden, September 2017



List of Symbols

Symbols and abbreviations used in the report

Ω	Angular spatial frequency	rad/m
ω	Natural Frequency	Hz
Ω_0	Reference angular spatial frequency	rad/m
$\Phi(z)$	Power spectral density of vertical displacements	m^3
<i>ADAMS</i>	Automated Dynamic Analysis of Mechanical Systems	
<i>BiW</i>	Body in White	
C	Unevenness parameter	$rad^{w-1} \cdot m^{3-w}$
c	Spring Stiffness	N/m
F_s	Sampling frequency	Hz
<i>FE</i>	Finite Element	
<i>FEMFAT</i>	Finite Element Method Fatigue	
<i>fft/FFT</i>	Single sided fast fourier transforms	
$G_d(\Omega)$	Power spectrum	m^3
$G_d(\Omega_0)$	Unevenness Index	m^3/rad
k	Stiffness Matrix	N/m
<i>LCA</i>	Lower control arm	
m	Mass Matrix	kg
<i>MBD</i>	Multi-Body Dynamics	
N	Number of data points in the total road length	
<i>NASTRAN</i>	FE Code	
<i>Pac2002(3DEnv)</i>	MF-Pacejka 2002 with 3D enveloping	
<i>PSD</i>	Power Spectral Density	
u	Mode Shapes	m
w, w_n	Waviness parameter describing the state of road deterioration	
$z(x)$	Vertical displacements along the longitudinal displacement x	m

Contents

List of Figures	xvii
List of Tables	xix
1 Introduction	1
1.1 Background	1
1.2 Purpose and Objectives	2
1.3 Method	2
1.4 Limitations	5
2 Vehicle modeling	7
2.1 Modal Analysis	7
2.2 Craig Brampton Reduction	8
2.3 Flexible Bodies in ADAMS	10
2.4 Vehicle Life Calculation	10
2.5 Vehicle Suspension System	11
2.6 ADAMS/Car and FEM vehicle model	15
2.6.1 Vehicle Model	16
3 Tyre modeling	21
3.1 Introduction	21
3.1.1 3D enveloping contact model	21
3.2 FTire	22
3.2.1 Mechanical model	22
3.3 PAC2002 with belt dynamics	23
3.3.1 Mechanical modeling	24
3.4 UA tire model	25
4 Road Profile modeling	27
4.1 Introduction	27
4.2 Road Classification	27
4.3 OpenCRG	28
4.4 Modeling Process	29
4.5 Road modeling Fundamentals	30
4.5.1 Power Spectral Density	30
4.5.2 Road profile spectrum	30
4.5.3 Kernel	32

4.6	Stochastic road modeling	33
4.6.1	Rough road modeling	33
4.6.1.1	Hybrid rough road model	33
4.6.1.2	Hybrid multi-variate rough road model	38
4.6.2	Belgian road modeling	40
4.6.3	Validation of Road Models	42
4.7	Deterministic Road modeling	45
4.7.1	Pothole, Curb and Bumps	46
4.7.2	Washboard	47
5	Results	49
5.1	Modal Analysis of Body-in-White (BiW)	49
5.2	Dynamic Simulations for Stress Calculations	51
5.2.1	Curb Impact Load case	51
5.2.2	Pothole Load Case	53
5.2.3	Rough Road Load Case	55
5.2.4	Stress on the LCA - Rough Road	56
6	Conclusion	59
7	Future Work	61
	Bibliography	63
A	Appendix 1	I
A.1	Body-in-White global mode shapes	I
A.1.1	Without Windshields	II
A.1.2	With Windshields	III
A.2	LCA mode shapes	IV
A.3	Damper Characteristics	V
A.4	Step size influence on normal tire forces - MF-Pacejka 2002 (3D Enveloping)	V

List of Figures

1.1	Approaches to Virtual Durability Testing	3
1.2	Detailed Workflow	4
2.1	Vibrating Full Vehicle Model [24]	7
2.2	Dependent Suspension Systems [25]	12
2.3	Independent Suspension Systems [25]	12
2.4	Semi-Dependent Suspension Systems [25]	13
2.5	Bushing Characteristics and Mounting Location. The bushings consists of an outer sleeve 3 and an inner sleeve 1 , with an rubber layer 2 in between. [26]	13
2.6	Linear Coil Spring Characteristics [27]	14
2.7	Damper and its characteristics [27]	14
2.8	ADAMS/Car Model Hierarchy	15
2.9	Front Suspension Evolution	17
2.10	Rear Suspension Evolution	17
2.11	Flexible MacPherson Front Suspension System from the ADAMS/Car Model	18
2.12	Flexible Twist Beam Rear Suspension System from the ADAMS/Car Model	18
2.13	Vehicle FEM Model	19
2.14	Rigid Vehicle Model	19
2.15	Flexible Vehicle Model	19
3.1	3D enveloping contact [35]	22
3.2	Bending Stiffness	23
3.3	PAC2002 belt dynamics model [37]	24
4.1	Signal classification	27
4.2	Curved regular grid representation [16]	28
4.3	Curved reference line [16]	28
4.4	Road modeling process	29
4.5	ISO classification of roads [18]	31
4.6	Shape of the kernel function 4.13	36
4.7	Hybrid Process: Top- Normalized Gaussian model; Middle- LMA model; Bottom- Combined Hybrid model	37
4.8	Hybrid uni-variate model (Road class C)	39
4.9	Multi-variate 3D road elevation mesh	39

4.10	Hybrid multi-variate model (Road class 3)	40
4.11	Belgian road model	41
4.12	Belgian road top view	41
4.13	Hexagonal Belgian blocks	42
4.14	Belgian road lateral profile	42
4.15	PSD of Hybrid uni-variate road model (Road class A, C, E, G)	43
4.16	PSD of Hybrid uni-variate road model (Road class B, D, F, H)	44
4.17	PSD of Hybrid multi-variate road model (Road class A, C, E, G)	44
4.18	PSD of Hybrid multi-variate road model (Road class B, D, F, H)	45
4.19	PSD of Belgian road model (Road class C)	45
4.20	Non-periodic road models	46
4.21	Periodic road models	47
5.1	Modal Analysis With and Without windshields	49
5.2	Modal Analysis With and Without Masses	50
5.3	The vehicle going over a road with a curb	51
5.4	Normal Force on the Left Front Tires	52
5.5	Fast Fourier Transform of the normal forces (Curb Impact)	52
5.6	The vehicle going over a road with potholes	53
5.7	Normal Force on the Left Front Tires	53
5.8	Fast Fourier Transform of the normal forces (Pothole Impact)	54
5.9	The vehicle going over a rough road	55
5.10	Fast Fourier Transform of the normal forces (Rough Road Impact)	55
5.11	Fast Fourier Transform for Mode 7	56
5.12	Fast Fourier Transform for Mode 9	56
5.13	Fast Fourier Transform for Mode 12	57
5.14	Stress distribution on the LCA when the vehicle going over a rough road	57
5.15	Stress distribution on the LCA - Comparison between dynamic and quasi-static simulations [5]	58

List of Tables

2.1	Number of Modes in the flexible vehicle model	17
4.1	Hybrid model parameters	38
4.2	ISO degree of roughness [18]	38
4.3	Modified ISO roughness values	40
4.4	Belgian road model parameters	43
5.1	Experimental and Theoretical Modal Analysis Without windshields .	50

1

Introduction

1.1 Background

A car is akin to a human body, highly complicated and immensely fascinating to study. Developing a car involves advanced engineering know-how and various teams working together to develop a finished product. Developing a vehicle in the highly competitive and consumer oriented market of the 21st century and at the same time providing high product quality is a demanding and challenging task.

The current trend in the automotive industry is towards Virtual Product Development (VPD) with a goal to eliminate physical testing in the development of automobiles. Volvo Car Group of Sweden and the General Motors of the United States of America have already outlined their vision for the year 2020 whereby they hope to completely develop a car from scratch through Computer Aided Engineering (CAE) [2]. This thesis would be a step in that direction of eliminating physical prototypes in the vehicle development cycle.

In course of usage of the vehicle, the input to the vehicle from the road disturbances cause loads and stresses to act on the vehicle parts. The life of the vehicle parts is determined by the magnitude and the type of the loads acting on it. Vehicle durability is one of the many important aspects of vehicle development. The physical durability testing is a long and time consuming process where the vehicle is driven on different types of roads on the test tracks for a considerable period of time until the part under investigation is damaged. With increasing competition, shorter product life cycle, the demand on the automotive industry to reduce the vehicle development cycle is increasing day-by-day. This gives impetus to the Computer Aided Engineering (CAE) in vehicle development.

Multi-Body Simulation (MBS) using elastic bodies have been frequently used to determine the time dependent loads of the flexible vehicle structure. These loads are then subsequently used for a succeeding FE analysis to obtain the stresses on the vehicle body. Some of these methods are explored in [3] [4] [5]. It is found that this method has quite a few disadvantages:

- Since the FE analysis is based on quasi static calculations, quasi static computation is conducted at every time step with the loads obtained from the dynamic MBS simulations. Therefore, the vibrational effects are neglected.

For complex vehicle components, this approach might produce errors.

- It has been found that every time step should be provided with the data from a full quasi static solution. For large FE structures and time series, this method becomes impractical.
- Dynamic simulation for a single pothole load case has been conducted by obtaining the peak loads on flexible bodies from MBS simulations and applying it into an quarter model of suspension system using the FE code RADIOSS [4] [6]. It has been found that these methods take a lot of time and money and are not practical for full vehicle simulations.

But little research has been carried out in the field of durability testing using modal superposition. Previous studies [9] [10] show that this method has numerous advantages as compared to the quasi static analysis using FE. Some of them are given below:

- It enables complete dynamic simulations of a fully flexible vehicle body incorporating all the properties of an FE model.
- Large time steps of the order of 20000 is possible with a vehicle body having 300000 nodes.
- Effect of vibration could be included, which is not possible in quasi static simulations.
- Full vehicle simulations of a fully flexible model having approximately 300 modes for each part on high frequency rough roads using highly fidelity tire models such as FTire, RMOD-K for the simulation time of 40secs and time steps of the order 0.001 would take approximately 20-24 hours. The subsequent stress calculation could be conducted in a very less time using FEMFAT, thus eliminating FE analysis for stress computation and lifetime calculation.

1.2 Purpose and Objectives

This thesis aims to study the durability and stress distribution of a fully flexible passenger vehicle model through complete dynamic analyses using MBD simulations. The concept of modal superposition and modal stress recovery is used to determine the stresses on the vehicle components. Virtual roads are created to provide input loads and forces to the vehicle model. With increasing software and hardware capabilities day-by-day, it is found that this method is highly suited for vehicle and component life time prediction during the initial concept phase.

1.3 Method

This work was preceded by a literature study of the current trends in physical and virtual durability testing of a vehicle and virtual road construction. Some of these

trends are given in [3] [4] [17].

The common approaches to virtual vehicle durability testing have been shown in the figure 1.1.

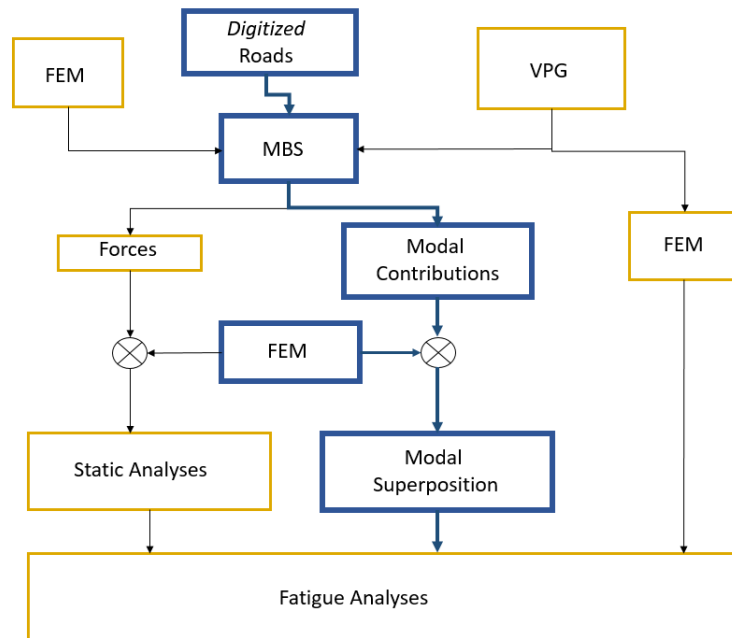


Figure 1.1: Approaches to Virtual Durability Testing

Initially, the work started with developing the full vehicle rigid body model of the passenger car in the MBS package ADAMS/Car with an already existing FEM model as reference. Modal analysis and condensation of the FEM model was performed in MSC Nastran to obtain the flexible bodies of all the vehicle components. Then, the rigid bodies in ADAMS/Car were replaced with flexible bodies. Accurate models of damper, springs and bushes are implemented [26] [7] [8]. Subsequently, virtual roads were created using OpenCRG and MATLAB. Different road types which are commonly used in durability testing were created virtually. The vehicle was then simulated at a speed of 50kmph on the created roads. The final roads which were chosen for simulation were Pothole 660mm length x 70mm depth, Rough Road Class 3 and Curb 90mm height. The modal coordinates of the left lower control arm (LCA) are then obtained. The modal coordinates of the modes which contribute highest to that particular disturbance are chosen. Then they are combined with the stress information obtained from the previous FE analysis conducted in NASTRAN and provided as the input to FEMFAT. The final stress distribution on the LCA for the dynamic maneuver is then obtained from FEMFAT analysis. The forces acting on the tires for different integration step sizes are compared to arrive at the requisite integration step size. The influence of different tire models on the forces acting on the components are compared to arrive at the ideal tire model suitable for durability analyses. The created road models are then validated by comparison of their PSD spectra with PSD spectra of the test data and the ISO standards [26].

1. Introduction

A unique method has been implemented to model the Belgian block roads by considering the shapes, sizes and the roughness of the actual cobblestone blocks. Also, the spaces between the cobblestone blocks have also been modelled in both the longitudinal and lateral direction. The created roads have been validated by comparing them with the ISO standards.

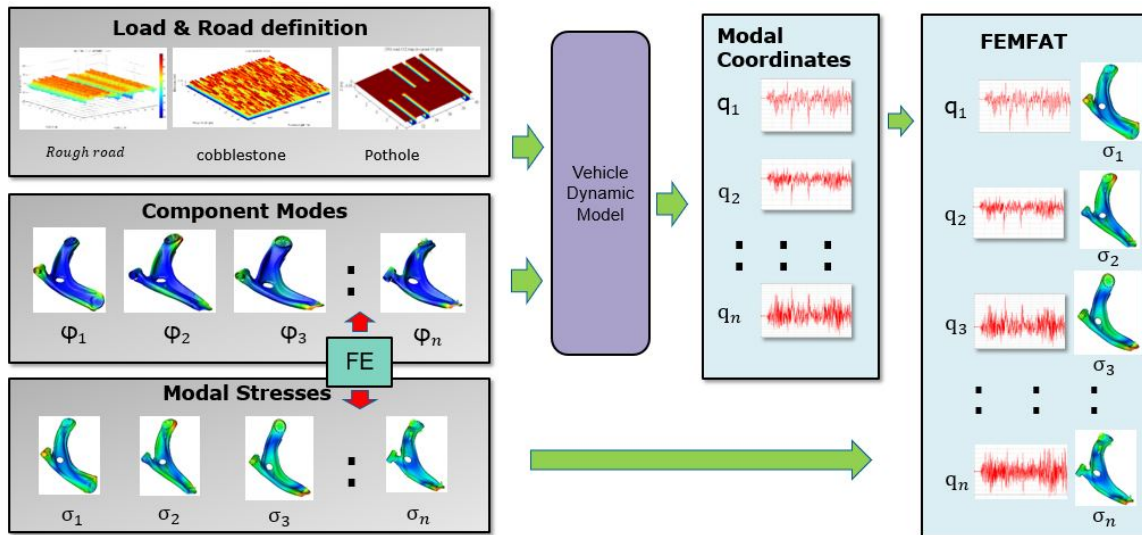


Figure 1.2: Detailed Workflow

1.4 Limitations

- The maneuvers performed in this thesis is limited to straight line analyses. Maneuvers on curved roads and cornering are not considered.
- The investigation on the type of FE model and their respective properties such as mesh size are not covered.
- The study is limited only to the investigation of the stress distribution on the components. The fatigue life of the components are not investigated.
- Due to the lack of test facilities and time constraint, physical testing and validation of the results have not been performed. Instead, the results have been compared with quasi static results from already existing literature.
- The component under study is limited to the left lower control arm (LCA) of the front suspension. The effects on the other suspension components and the vehicle body are not investigated.
- The parts such as doors, hood, boot and the exhaust pipe have been excluded from the vehicle model. The vehicle body is limited to just the BiW.
- The durability analysis of the vehicle subsystems such as transmission, engine and the parts therein are out of scope of this study.

2

Vehicle modeling

2.1 Modal Analysis

Vibrations of a system which is unforced and undamped are responses which depict their natural behavior. This type of system where no external forces act and no damping exists is known as a *free system*.

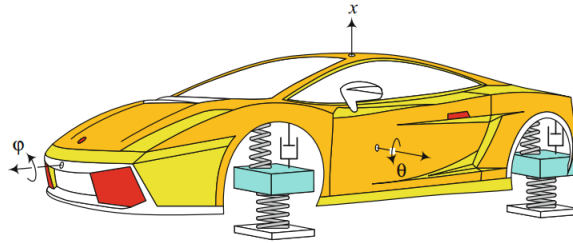


Figure 2.1: Vibrating Full Vehicle Model [24]

A system which is free is described by the following equations according to the Newton's law.

$$[m]\ddot{x} + [k]x = 0 \quad (2.1)$$

The response to this system is given as, which is the solution to the system:

$$x = \mathbf{u}_i \sin(\omega_i t) \quad (2.2)$$

Where, \mathbf{u}_i denotes the mode shapes, t gives the time and ω_i is the natural frequency $i=1,2,3,\dots,n$.

From equations (2.1) and (2.2), we obtain:

$$([k] - \omega_i^2 [m])\mathbf{u}_i = 0 \quad (2.3)$$

The above equation gives an n^{th} order eigenvalue problem for a system with n degrees of freedom.

Solving the above problem, we get n eigenfrequencies having eigenvectors \mathbf{u}_i . If the eigenfrequencies of the system are distinct, we obtain orthogonal eigenvectors with respect to their mass and stiffness matrices. From orthogonality, the following properties are obtained for the mass and stiffness matrices.

$$\mathbf{u}_i^T[m]\mathbf{u}_j = \begin{cases} 0, & \text{if } i \neq j \\ m_i & \text{if } i = j \end{cases} \quad \mathbf{u}_i^T[k]\mathbf{u}_j = \begin{cases} 0, & \text{if } i \neq j \\ k_i & \text{if } i = j \end{cases} \quad (2.4)$$

The eigenvectors are mass normalized by setting $m_i = 1$. This results in $\omega_i^2 = k_i$. Forming a matrix with mode shapes as columns gives:

$$\Psi = [\mathbf{u}_1, \mathbf{u}_2, \mathbf{u}_3, \dots, \mathbf{u}_n] \quad (2.5)$$

The above equation could be used to transform the physical coordinates into modal coordinates using the following equation:

$$x = \Psi q \quad (2.6)$$

Thus, the following equation describes the forced damping of Multi Degree of Freedom System (MDOF) where $F(t)$ gives the external force applied.

$$[m]\Psi\ddot{q} + [k]\Psi q = F(t) \quad (2.7)$$

Multiplying by Ψ^T we get:

$$\Psi^T[m]\Psi\ddot{q} + \Psi^T[k]\Psi q = \Psi^T F(t) \quad (2.8)$$

We can then write the above equation as:

$$[\hat{\mathbf{m}}]\ddot{q} + [\hat{\mathbf{k}}]q = \hat{\mathbf{F}}(t) \quad (2.9)$$

Since the mass matrix (modal) $[\hat{\mathbf{m}}]$ and stiffness matrix (modal) $[\hat{\mathbf{k}}]$ are diagonal matrices, we could say that that the equations of motion has been decoupled successfully.

2.2 Craig Brampton Reduction

The Craig-Brampton Reduction method is one of the method to reduce the size of an finite element (FE) model. In multi-body simulations (MBS) interface nodes are the common boundary points where rigid or flexible boundary points are coupled together. For this application the modal approach has been found to be inadequate [11]. Therefore, a method known as component mode synthesis (CMS) has been developed. CMS is used for dynamic analysis of systems having differently connected subsystems. Some of the other methods are *Guyan Reduction* and *Modal Decoupling* [12]. In the C-B method, the boundary points are assumed fixed and their motion is combined with the modes of the structure [12].

The advantages of C-B approach compared to the other approaches mentioned above are as follows:

- It allows for the size of the problem to be reduced.
- Both the mass matrices and the stiffness matrices are accounted for even though the problem size is reduced.

- The size of the problem could be defined based on the required frequency ranges.
- It allows for the boundary conditions to be different at the interface.

Let us describe the system by *Newton's equation*:

$$[m]\ddot{x} + [k]x = F(t) \quad (2.10)$$

Dividing the system into interior DOFs x_I and boundary DOFs x_B , we get:

$$\begin{bmatrix} m_{BB} & m_{BI} \\ m_{IB} & m_{II} \end{bmatrix} \begin{bmatrix} \ddot{x}_B \\ \ddot{x}_I \end{bmatrix} + \begin{bmatrix} k_{BB} & k_{BI} \\ k_{IB} & k_{II} \end{bmatrix} \begin{bmatrix} x_B \\ x_I \end{bmatrix} = \begin{bmatrix} F_B \\ F_I \end{bmatrix} \quad (2.11)$$

In the above equations, **I** and **B** depict *interior* and *boundary* respectively. The notation m_{IB} denote mass-coupling between interior and boundary DOFs and m_{BB} denote the mass-coupling between boundary DOFs. The interior DOFs are described by combining *constraint modes*- obtained by unit displacement of each boundary DOF and *fixed boundary normal modes*- obtained by computing the eigensolution of the interior DOFs with the boundary DOFs fixed.

$$([k_{II}] - \omega^2[m_{II}])\mathbf{u}_{II} = 0 \quad (2.12)$$

By reduction and retaining the requisite number of modes 'n', we obtain the matrix with normal modes for the interior DOFs as:

$$\Psi_I = [\mathbf{u}_{II1}, \mathbf{u}_{II2}, \mathbf{u}_{II3}, \dots, \mathbf{u}_{II n}] \quad (2.13)$$

Assuming zero inertial effects for the static modes and providing unit displacement for each boundary DOF, the constraint modal matrix Ψ_B could be calculated. Therefore, the C-B transformation matrix giving the relationship between C-B coordinates and the physical coordinates is obtained.

$$\begin{bmatrix} x_B \\ x_I \end{bmatrix} = \begin{bmatrix} I & 0 \\ \Psi_B & \Psi_I \end{bmatrix} \begin{bmatrix} q_B \\ q_I \end{bmatrix} = \Psi_{CB}q_{CB} \quad (2.14)$$

Where the identity matrix is denoted by the letter I . From substituting the equation (2.14) into the equation (2.10), and multiplying with Ψ_{CB}^T , the original system is reduced by C-B method.

$$\Psi_{CB}^T[m]\Psi_{CB}\ddot{q}_{CB} + \Psi_{CB}^T[k]\Psi_{CB}q_{CB} = \Psi_{CB}^T F(t) \quad (2.15)$$

Rewriting the above equation:

$$[m]_{CB}\ddot{q}_{CB} + [k]_{CB}q_{CB} = F_{CB}(t) \quad (2.16)$$

Here, the blocks of $[m]_{CB}$ and $[k]_{CB}$ which are associated with the eigenvectors Ψ_I are diagonal and $[k]_{CB}$ is block diagonal matrix.

2.3 Flexible Bodies in ADAMS

Even though the C-B method provides a reduced model allowing coupling between other substructures and capturing the dynamic properties of the system, the C-B method has certain shortcomings for successful dynamic simulation in ADAMS. Some of the reasons are [11]:

- The C-B modes contain six rigid body modes which should be eliminated as the rigid body DOFs are provided by ADAMS.
- Static condensation is performed to obtain the *constraint modes*. Therefore, they don't have natural frequency associated with them.
- Therefore, disabling the constraint modes is equivalent to applying a constraint on the system.

The C-B system is orthogonalized by solving the below equation:

$$([k_{CB}] - \lambda^2[m_{CB}])\mathbf{u}_{CB} = 0 \quad (2.17)$$

The eigenvectors so obtained is arranged into a transformation matrix T . Using $q_{CB} = Tq^o$, the system is transformed to be orthogonal.

$$T^T[m_{CB}]T\ddot{q}^o + T^T[k_{CB}]Tq^o = T^T F(t) \quad (2.18)$$

A diagonal system is obtained from this transformation. The static *constraint modes* are transformed into boundary eigenvectors with a corresponding eigenfrequency. The fixed boundary normal modes are converted into modes which approximate the unconstrained modes of the system. Additionally, a set of modes are generated which cannot be interpreted in terms of physical eigenvectors. Therefore:

- The diagonal system now has six *rigid body modes* which could be disabled.
- Each mode has a corresponding natural frequency associated with them. Therefore, static *constraint modes* are eliminated.
- The boundary modes could also be disabled without constraining the system but certain mode shapes would not be visible.

Therefore, the flexible bodies are described by the obtained linear system in MSC ADAMS, which are in turn suitable for dynamic simulations .

2.4 Vehicle Life Calculation

FEMFAT is a program for fatigue and strength analysis of statically and dynamically loaded components on the basis of the finite element (FE) analysis results [28]. The FEM results are analyzed based on experimental and theoretical research, model trials and operational experience. The procedure for the strength and fatigue analysis is based on the *influencing quantities method* which is described in the TGL standard (Technische Güte und Lieferbedingungen) and the FKM guidelines (Forschungskuratorium Maschinenbau). The Local S/N curves are calculated at the

FEM nodes which are influenced by the local component properties and loads, on the basis of unnotched sample strength data [28].

FEMFAT uses the *critical plane* approach to analyze the stress and strain experienced by a material plane. It also identifies the plane that is likely to experience the most extreme damage. *Critical plane* analysis is used widely in engineering analysis to analyze the influence of multi-axial and cyclic loading on the fatigue life of materials and structures [29].

The advantage of *critical plane* analysis is that it gives the damage of a component in specific material planes. Therefore, multiple out-of-phase load inputs could be treated with high accuracy. This method could also be adapted to different materials [29].

2.5 Vehicle Suspension System

Vehicle Suspension is a mechanism that connects the wheels of a vehicle to the body or to the frame attached to the vehicle body. The suspension deformation with structural deformation plays an important role in vehicle handling and ride comfort by allowing for appropriate camber angle changes during dynamic maneuvers.

The basic functions of suspension systems are:

- Segregate the vehicle body from road vibrations and forces which would otherwise be transferred to the vehicle occupants.
- Maintain the road grip between the tires and the road surface by facilitating the contact between the road and the tires at all times.
- Facilitate load transfer during dynamic maneuvers.
- Maintain the alignment of the wheels of the vehicle and allow for dynamic changes in camber during vehicle maneuvers.

Suspensions are classified into different types according to their functional requirements as below:

- **Dependent Suspension:** The dependent suspensions are characterized by a rigid link between the two wheels of an axle. The motion of one wheel affects the other wheel as well due to the rigid coupling between the wheels. The dependent suspensions are commonly used on heavy vehicles such as trucks and buses. These types of suspension systems are also referred to as rigid axle suspension systems.
- **Independent Suspension:** These types of suspension systems, as opposed to the dependent types of suspension systems, allow separate movement of wheels of the same axle relative to the vehicle body. Therefore, the compression/jounce of one wheel does not affect the motion of the other wheel. Reduced sprung mass, sufficiently large amount of elastokinematic and kinematic design freedom are some of the advantages of independent suspension

2. Vehicle modeling

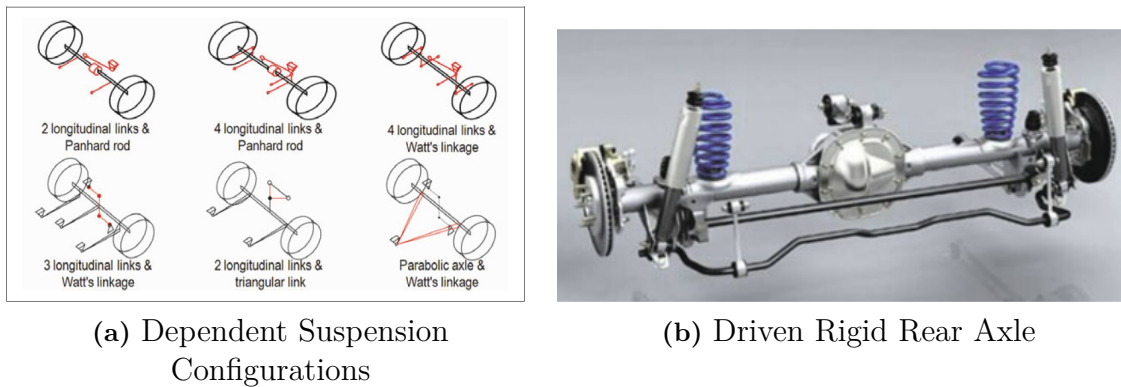


Figure 2.2: Dependent Suspension Systems [25]

systems. Commonly, the independent suspension systems are made of multiple individual links that constrain five out of six degrees of freedom of the wheel.

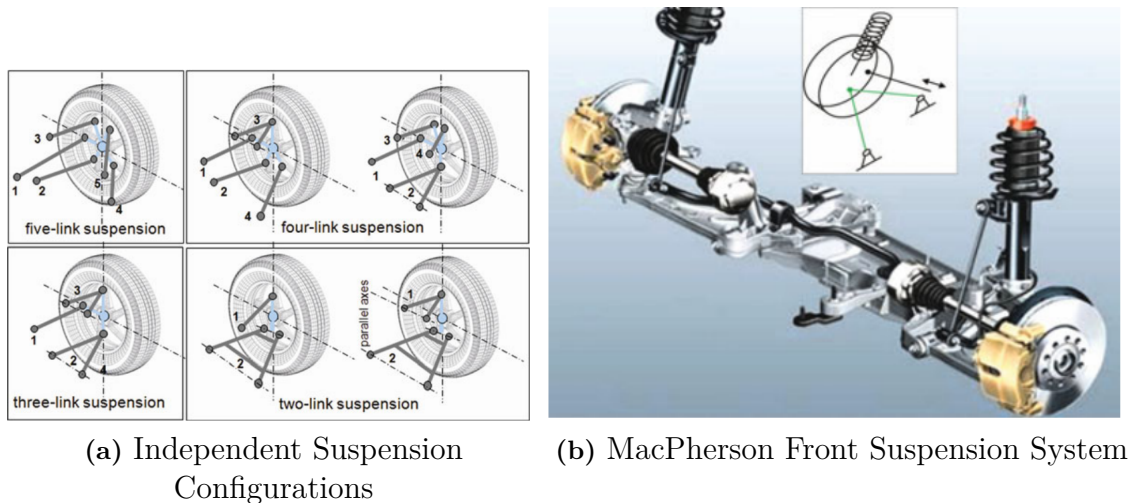


Figure 2.3: Independent Suspension Systems [25]

- Semi-Dependent Suspension System:** Semi-Dependent suspension systems are also known as twist beam axles. These types of suspension systems have intermediate characteristics between dependent and independent suspension systems. The wheels of an axle are commonly connected with flexible beams known as twist axles. During parallel travel of the wheels, there is negligible changes in camber, track width and toe angle. But, during opposite wheel travel, this type of suspensions provide lower roll center and improved camber. Simple in construction, easy to assemble and disassemble are some of the advantages.

A vehicle suspension system consists of various parts such as bushings, joints, dampers and springs that provide the axle of a vehicle with their elastokinematic properties.

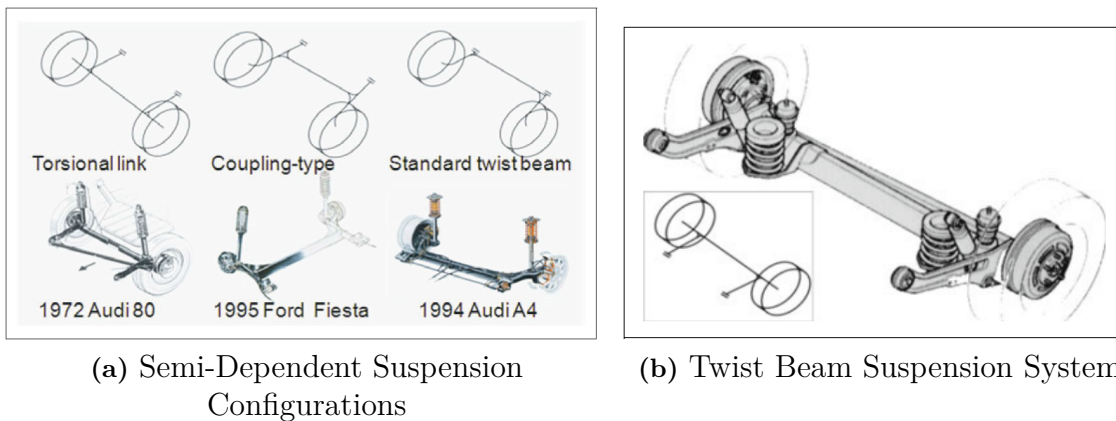


Figure 2.4: Semi-Dependent Suspension Systems [25]

- Elastic Bushings:** Rubber bushings due to their elastic nature allow relative movement of the control arm with reference to the vehicle body or the suspension subframe. The bushings are made up of a layer of vulcanized rubber sandwiched between two concentric metal sleeves. The rubber bushings are designed to provide the suspension with elastokinematic behaviour by the variation of toe angle and wheelbase. Bushings with *higher stiffness* will provide superior road grip and handling behaviour but will compromise the ride comfort. The bushings are typically characterized by their stiffness and damping in X , Y and Z directions along with their torsional stiffness and damping respectively (Figure 2.5).

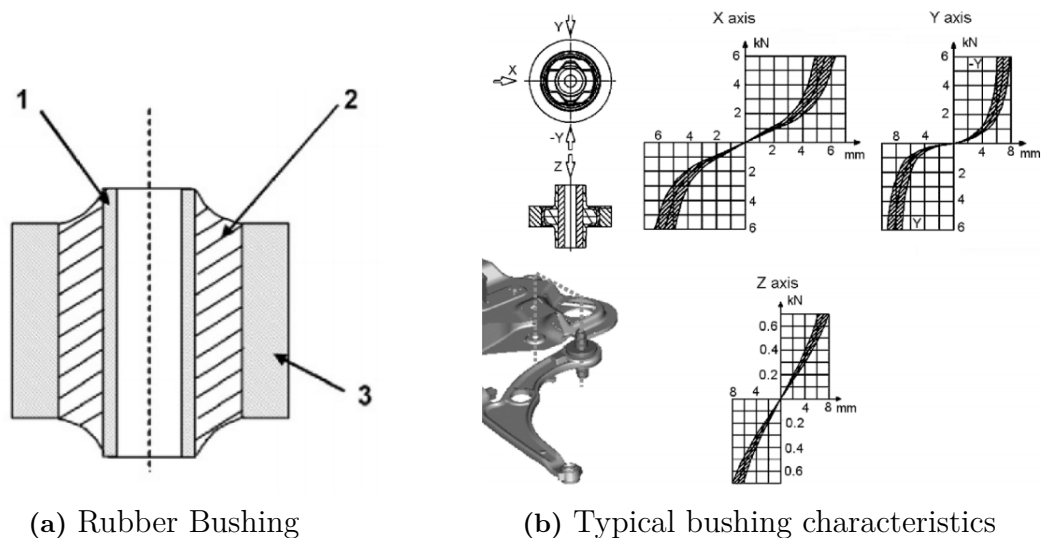


Figure 2.5: Bushing Characteristics and Mounting Location. The bushings consists of an outer sleeve 3 and an inner sleeve 1, with an rubber layer 2 in between. [26]

- Springs:** The springs support the vehicle weight. Different types of springs such as coil, leaf springs, air springs and torsion bars are used.

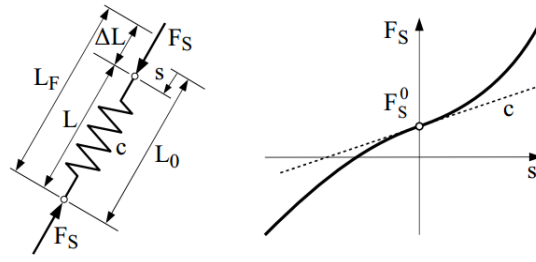


Figure 2.6: Linear Coil Spring Characteristics [27]

A linear coil spring is shown in the figure 2.6. It is characterized by its free length L_F and stiffness c . The force on the spring is then given by [27]:

$$F_s = c(L_F - L) = c\Delta L \quad (2.19)$$

Where, L denotes the actual length and ΔL gives the overall deflection of the spring. When mounted on the chassis, the spring compresses to support the weight of the chassis. Therefore, it will be compressed to a length $L_0 < L_F$. Hence, the above equation can be written as:

$$F_s = c(L_F - (L_0 - s)) = c(L_F - L_0) + cs = F_s^0 + cs \quad (2.20)$$

Here, F_s^0 denotes the spring preload and $s = L_0 - L$ gives the spring displacement from the configuration length of the spring.

- **Dampers:** Dampers or Shock Absorbers are used to damp out the roll, pitch motion and the oscillations caused by the road input on to the vehicle. The dampers used in the vehicles are oil pumps with orifices provided in the piston and the chamber. During the suspension travel the fluid is forced through the orifices, thus 'damping' or slowing down the oscillations caused by the vehicle moving over the road obstacles.

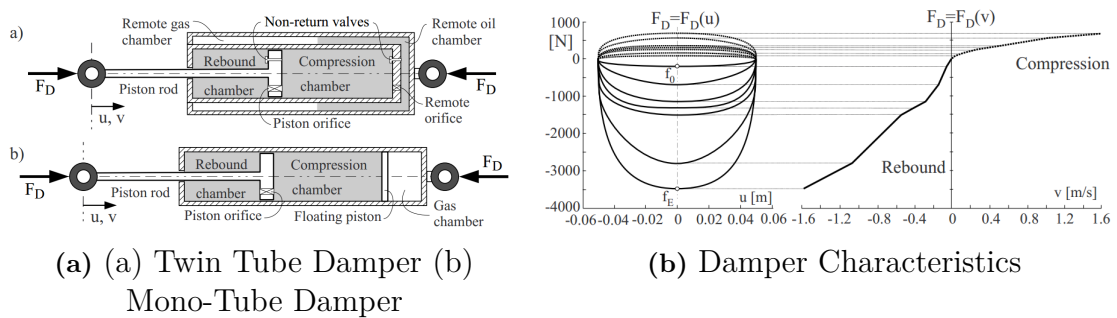


Figure 2.7: Damper and its characteristics [27]

In vehicle dynamic applications the damper is characterized by [27]:

$$F_D = F_D(v) \quad (2.21)$$

The above equation is used to obtain the damper force F_D as a function of damper compression velocity $v = \dot{u}$. The characteristics are obtained by exciting the damper with a sinusoidal signal $u = u_0 \sin 2\pi ft$. The frequency is varied in different steps of f_0 to f_E , force vs displacement curves $F_D = F_D(u)$ are obtained. The peak values of force are taken at $u = 0$ to generate the damper curve as shown in the figure 2.7 [27].

- **Steering Ball Joint:** The lower control is connected to the suspension strut/the wheel carrier through a spherical joint known as the *steering knuckle*. The joint is highly stiff in every direction except the radial direction.

2.6 ADAMS/Car and FEM vehicle model

ADAMS/Car is multibody software for modeling vehicles. It allows the user to create virtual models and prototypes and perform realistic analysis. It also allows the user to create highly complex models and perform complex dynamic maneuvers. The model hierarchy in the ADAMS/Car suite of products are as shown below:

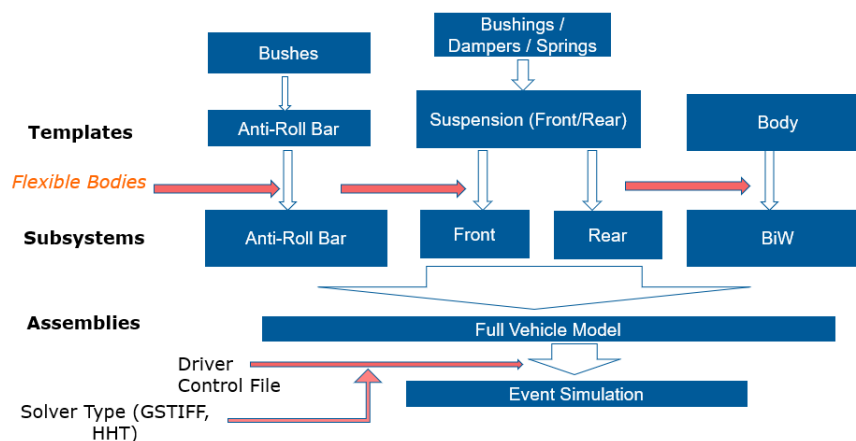


Figure 2.8: ADAMS/Car Model Hierarchy

A vehicle model in ADAMS/Car is categorized as shown in the figure 2.8. It is made of Templates, Subsystems and Property Files.

- **Templates:** Templates are parametric models that are built by expert users within the template builder. Default geometric data such as connection points of a suspension system, topology of the models and characteristics of forces elements such as dampers and bushes are defined inside a template.
- **Subsystems:** Subsystems are based on the templates. The subsystem of a vehicle part references to a template that defines the subsystems construction, including the type of parts and how the parts interact and attach to one another. Subsystems allow the standard users to modify the parametric information of some of the components such as hard points of the suspension system and properties of bushes and dampers. But, subsystems do not allow

the modification of other parametric information such as orientation of the components.

- **Property Files:** The property files are ASCII-based files that contain data for modeling components such as bushings, dampers and springs.

2.6.1 Vehicle Model

The car model consists of a *MacPherson* front suspension system and a *Twist Beam* rear suspension system. The ADAMS/Car model consists of flexible bodies implemented. The vehicle model is fully flexible i.e., the control arms, subframe, the steering tie-rods and the vehicle body-in-white (BiW) are flexible imported after condensation from an existing FEM vehicle model.

The difference between the FEM model and the ADAMS/Car model is that the parts such as windshields, exhaust pipe, doors and seats have not been considered.

The following procedure was followed to build up the full vehicle model in ADAMS/Car:

- Obtain the suspension *hardpoints* from the FEM vehicle model.
- Build up *rigid* full vehicle model in ADAMS/Car using the suspension hardpoints obtained from the FEM model.
- Perform FE condensation and modal analysis in MSC NASTRAN to obtain the *flexible* bodies by appropriately choosing the range of natural frequencies for a particular component.
- Replace the *rigid* vehicle components with the *flexible* bodies to build up the fully *flexible* vehicle model in ADAMS/Car.

The vehicle parts and the total number of modes associated with them are given in the following table (Table 2.1).

Table 2.1: Number of Modes in the flexible vehicle model

Part	Number of Modes
Left and Right LCA	318
Left and Right Strut	330
Subframe	426
Left and Right steering Tierod	318
BiW	558
Rear Axle	360

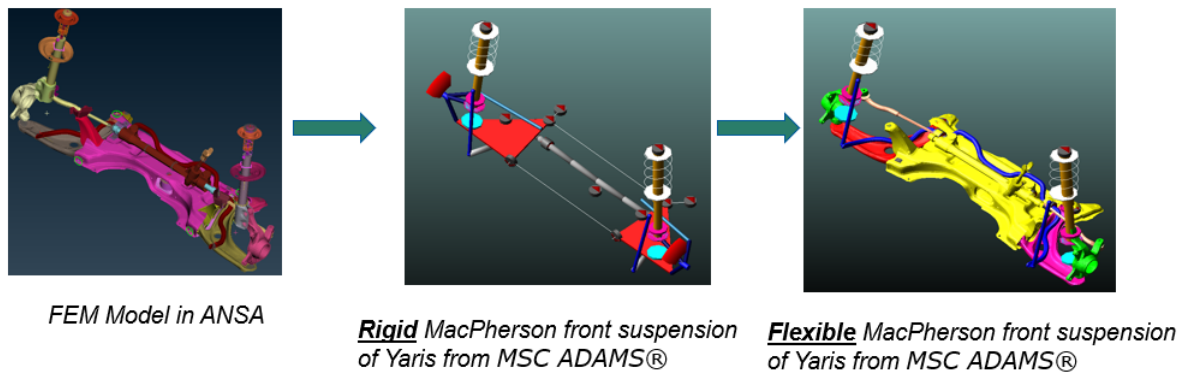


Figure 2.9: Front Suspension Evolution

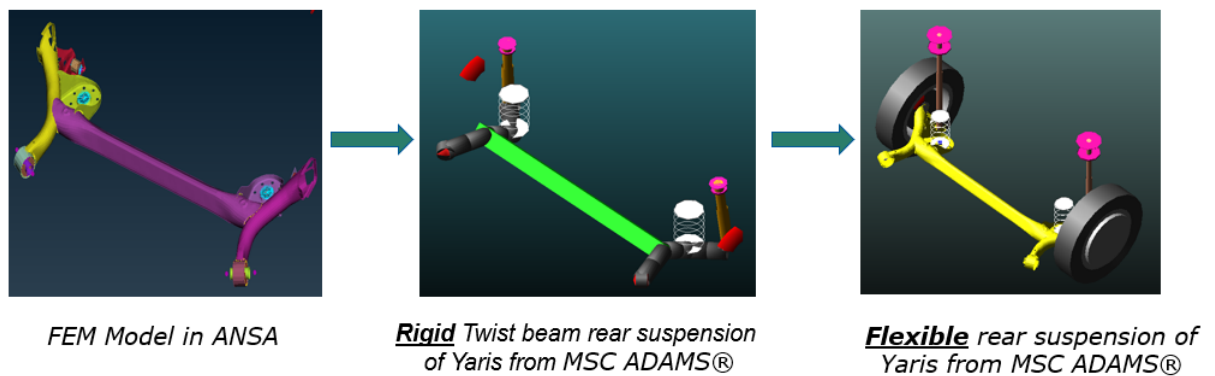


Figure 2.10: Rear Suspension Evolution

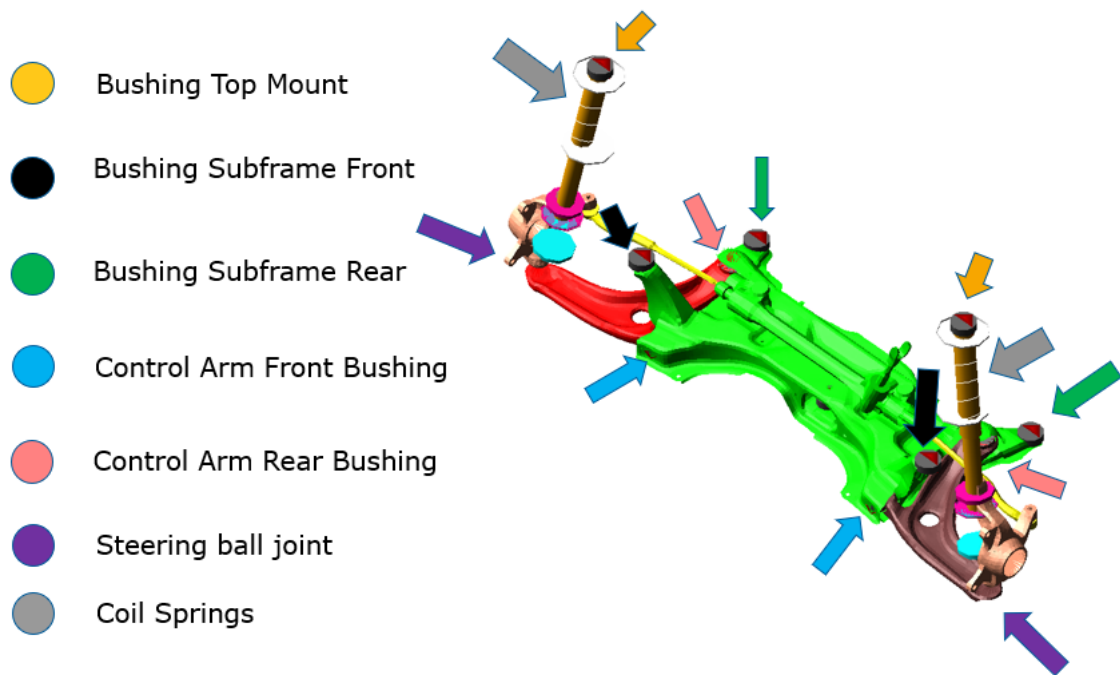


Figure 2.11: Flexible MacPherson Front Suspension System from the ADAMS/Car Model

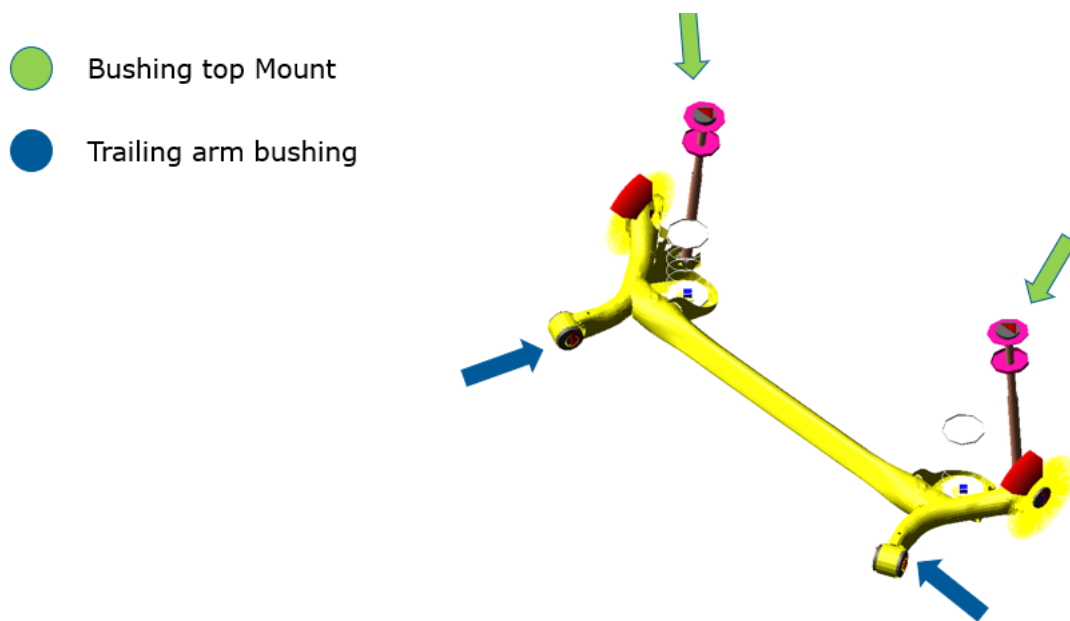


Figure 2.12: Flexible Twist Beam Rear Suspension System from the ADAMS/Car Model

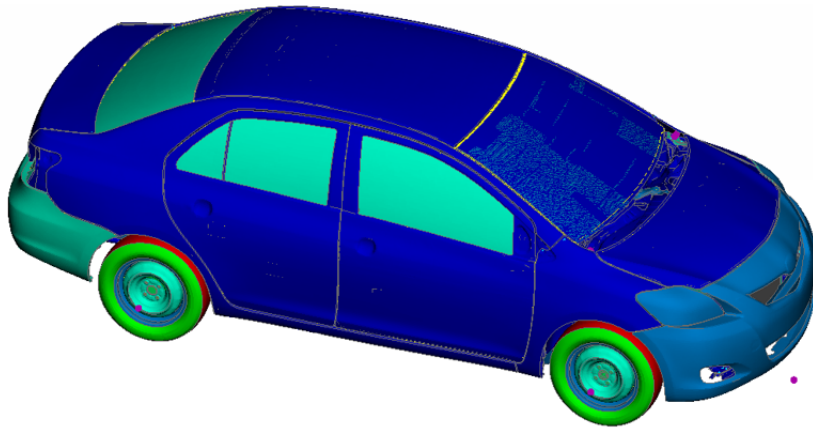


Figure 2.13: Vehicle FEM Model

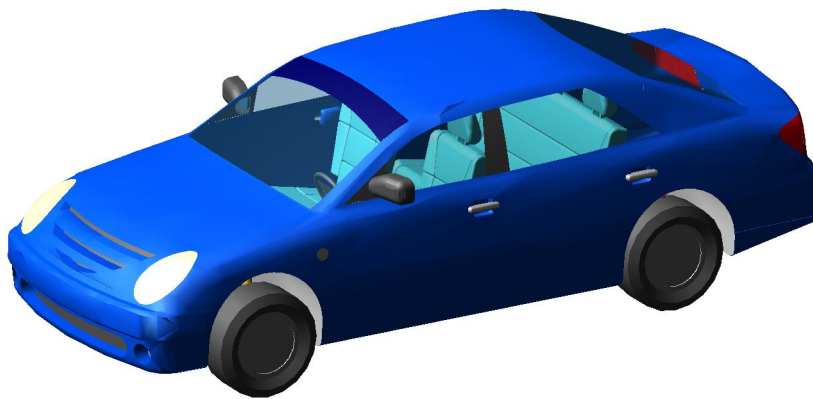


Figure 2.14: Rigid Vehicle Model



Figure 2.15: Flexible Vehicle Model

3

Tyre modeling

3.1 Introduction

Most vehicle dynamics applications especially durability and ride simulations requires an accurate knowledge of tire-road interaction forces because the movements of a vehicle primarily depend on the road forces on the tires. These interaction forces depend on both road and tire properties, and the motion of the tire with respect to the road. For durability the accurate estimation of normal force becomes relevant compared to other tire forces and therefore we primarily focus on how the normal forces are computed by different tire models.

Durability simulations require 3D contact analyses for stress and fatigue studies, which require component force and acceleration calculation. These studies can be used to estimate the effects of road profiles, such as pothole, curb, or Belgian block. Therefore choosing a proper tire model becomes crucial and using an improper tire model can result in non-realistic analysis results [35].

For durability analysis Adams tire offers FTire, PAC2002 (with belt dynamics), UA and 521 tire models. We have chosen to use FTire, PAC2002 and UA tire models as they support 3D enveloping contact method and allows for simulations on CRG roads. Here we compare the effects of these tire models on durability of the Lower Control Arm (LCA) when subjected to various durability tests.

3.1.1 3D enveloping contact model

The 3D Enveloping Contact method is used for driving over obstacles having wavelengths shorter than the tire contact patch and it is compatible with all Adams tire models other than FTire (no selection required) and 521 tire model (uses penetrated volume contact method [35]).

It is used for predicting the nonlinear enveloping behavior of a tire using a semi-empirical 'tandem cam' approach in which a series of connected elliptical cams are defined whose shape at the contact patch correspond to the outside tire contour. During the simulation the contact of each cam with the road is determined. Then the sum of the position and orientation of all cams results in an effective height, effective slope, effective road curvature and effective road camber for the tire model. The 3D version of this method has been used, so that obstacles that are not symmetric with respect to the wheel will result in an effective road camber input for the tire

model. The picture below shows the position of the cams for a tire rolling over a step obstacle [35].

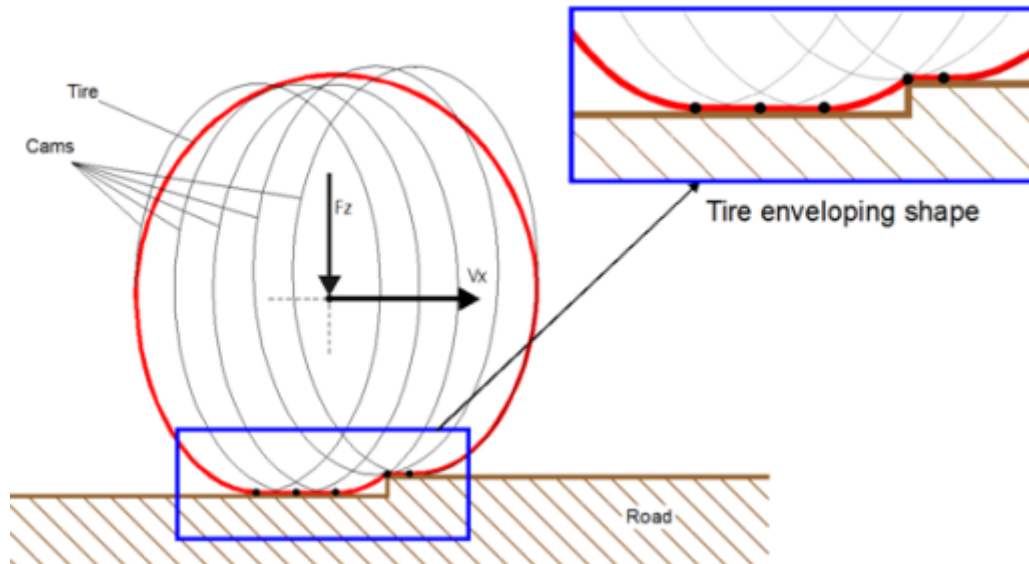


Figure 3.1: 3D enveloping contact [35]

3.2 FTire

FTire (Flexible ring tire model), It is a non-linear vibrational tire model which can be used in ride, comfort and durability simulations, even on high frequency rough roads.

The main advantages of FTire are:

- Fully nonlinear and accurate at frequencies up to 200 Hz [33].
- Valid for obstacle wave lengths less than half the length of the contact patch.
- Accurately simulates when passing single obstacles, like cleats and potholes.
- Applicable to situations like misuse of tires and sudden pressure loss.
- Compared to other tire models, FTire resolves road irregularities without any pre-processing of the road data.

3.2.1 Mechanical model

The tire belt is modelled as an extensible and flexible ring having bending stiffness with dynamic stiffness in radial, tangential, and lateral directions, which are distributed elastically on the rim. The degrees of freedom is set up such that the movements of the ring both in-plane and out-of-plane are possible. The ring has a finite number of belt elements of discrete masses and this elements are coupled

to each other by stiff springs and by bending stiffness both in-plane and out-of-plane.

Each belt element has number (5 to 50) of mass-less ‘tread blocks’ located along several parallel lines to achieve the whole contact patch along the longitudinal and lateral road surface. The blocks carry nonlinear stiffness and damping properties in radial, tangential, and lateral direction. The radial deflections of the blocks depend on the road profile, location, and orientation of the corresponding belt elements. Tangential and lateral deflections are determined by the sliding velocity on the ground and the local values of the sliding coefficient.

Belt *In-Plane* bending stiffness of the tire model shown in the figure 3.2a is modelled by means of torsional springs about the lateral axis and the torsional deflection is given by the angle between three consecutive belt elements projected on to the rim’s mid plane. Belt *Out-plane* bending stiffness shown in the figure 3.2b is realized by means of torsional springs about the radial axis and angle between the three consecutive elements, projected on to the tangential plane gives the torsional deflection in radial direction.

FTire estimates all six components of tire forces and torques acting on the rim by integrating the forces in the elastic foundation of the belt. FTire can also consider the non-uniformity of the tire as well as static and dynamic imbalances in the tire [34, 33, 35].

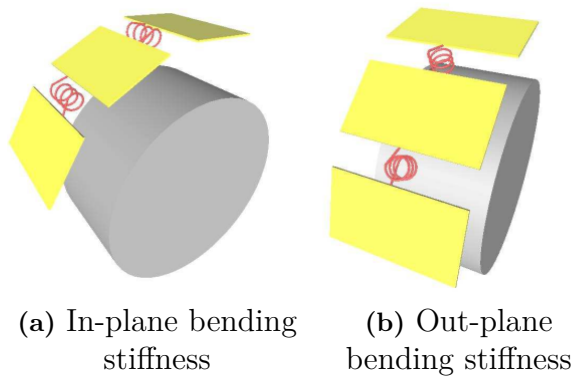


Figure 3.2: Bending Stiffness

FTire parameterization process is proposed in [33, 35] and it is best done by using the tool box FTire/fit (time- and frequency-domain parameter identification) or FTire/estim (qualified parameter estimation by comparison with a reference tire).

3.3 PAC2002 with belt dynamics

The PAC2002 is a Magic-Formula tire model (an empirical formulae describing the forces and moments from road on to tire) based on Tyre and Vehicle Dynamics by Pacejka [36] developed by MSC Software. Generally, a MF tire model is used

in vehicle handling and stability simulations. MF tire model describes the tire behavior for smooth roads (road obstacle wavelengths longer than the tire radius) up to frequencies of 8 Hz. However the PAC2002 has extended functionality that increases the validity towards short road obstacle wavelengths (with use of the 3D Enveloping Contact) and higher frequencies (up to 70 - 80 Hz) by using the tire belt dynamics modeling [35].

3.3.1 Mechanical modeling

At frequencies higher than 15 Hz the dynamics of the tire belt has a considerable effect on the durability of the vehicle or component. Figure 3.3 shows the PAC2002 belt dynamics model describing lowest eigen modes of the belt by assuming the belt as a rigid ring.

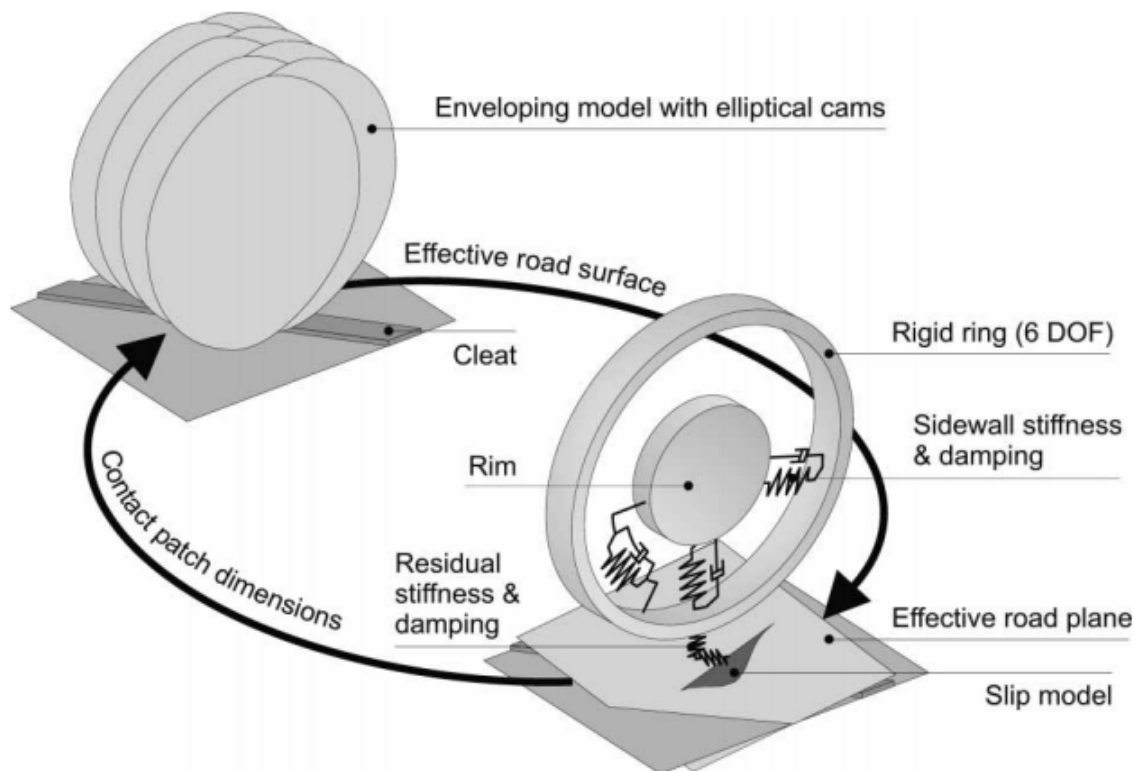


Figure 3.3: PAC2002 belt dynamics model [37]

The wheel - tire assembly has a rim part and a belt part with a six degree of freedom bushing in between them with stiffness and damping to allow the belt to move with respect to the rim. The overall vertical stiffness is corrected by adding a residual stiffness in between the belt and the road.

The spring deflection ρ and damper velocity $\dot{\rho}$ are derived with the (effective) road height, road angle and road camber information supplied by the 3D enveloping contact method.

$$\rho = R_0[q_{REO} + q_{V1}\left(\frac{\Omega R_0}{V_0}\right)^2] - R_1 \quad (3.1)$$

Where the tire rotational speed $\Omega = \frac{V_x}{R_e}$, R_0 is the free tire radius, R_1 is the loaded tire radius, V_x is the vehicle longitudinal velocity, q_{REO} is the correction factor for measured unloaded radius and q_{V1} is the tire radius growth coefficient.

Knowing the deflection ρ the normal force F_z can be estimated using the equation 3.2.

$$F_z = \left(q_{REO} + q_{V2} \left| \Omega \frac{R_0}{V_0} - (q_{Fcx1} \frac{F_x}{F_{z0}}) - (q_{Fcx1} \frac{F_x}{F_{z0}}) - (q_{Fcy1} \frac{F_y}{F_{z0}}) + q_{Fc\gamma 1} \gamma^2 \right) \right. \\ \left. \left[q_{Fz1} \frac{\rho}{R_0} + q_{Fz2} \left(\frac{\rho}{R_0} \right)^2 + q_{Fz3} \gamma^2 \frac{\rho}{R_0} \right] \left((1 + q_{Fz1} dp_i)_{Cz} F_{z0} \right). \quad (3.2)$$

Using this formula, the vertical tire stiffness increases due to increasing rotational speed and decreases by longitudinal and lateral tire forces.

The road-belt friction interaction forces are calculated with the Non linear transient model (contact mass approach) in combination the Magic Formula equations for the tire's Force Moment response. An in detailed modeling methodology can be found in Adams Tire documentation [35]. Running the PAC2002 with the belt dynamics option will leverage the validity range of the tire model towards up to 70 - 80 Hz frequency range.

3.4 UA tire model

The UA-Tire model (University of Arizona) calculates the longitudinal force F_x , lateral force F_y , normal force F_z , rolling resistance moment M_y and self aligning moment M_z at the ground contact point as a function of the tire kinematic states longitudinal slip κ , side slip α and camber angle γ , tire deflection ρ and deflection velocity $\dot{\rho}$. An in depth modeling of the UA tire model is explained in 38 and 35.

Normal Force F_z given by the equation 3.3 is calculated assuming a linear spring with stiffness k_z and damper with damping constant c_z .

$$F_z = k_z \cdot \rho + c_z \cdot \dot{\rho} \quad (3.3)$$

3D enveloping contact model provides the effective road height and road plane information to the tire to estimate deflection and penetration. If the tire loses contact with the road, the tire deflection and deflection velocity become zero so the resulting normal force F_z will also be zero [35].

4

Road Profile modeling

4.1 Introduction

The Virtual Proving Ground method for durability requires the virtual vehicle model to be driven on a digitized road. The VPG method uses road profile as the input to the vehicle model. Using this method, tests can be performed without any vehicle specific measured data, which is usually fed as the load input to the wheel spindles, where as the VPG method uses road elevations as the input at the tire-road contact patch [17].

4.2 Road Classification

Roads can be realized as models of deterministic and random signals as shown in the figure 4.1 and they are classified based on their signal types according to the list 4.2.

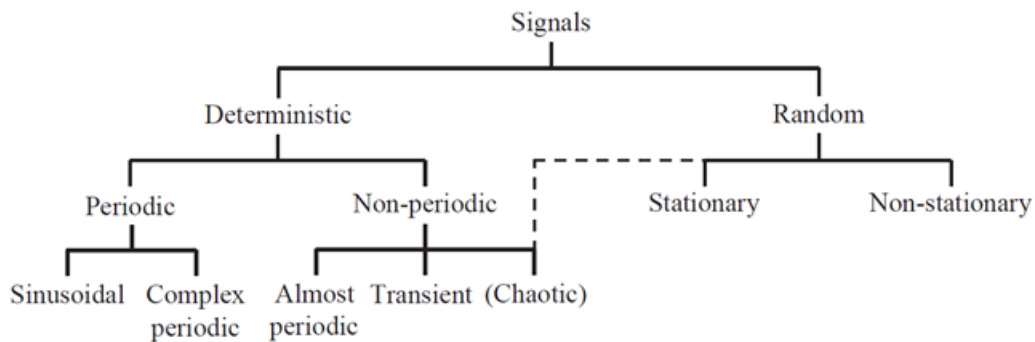


Figure 4.1: Signal classification

Classification of road models according to the signal types.

- Deterministic-Periodic-Sinusoidal signals.
 - Washboard In Phase
 - Washboard Out of Phase
- Deterministic-Non periodic-Single Event signals
 - Pothole road
 - Curb
 - Bumps and Ramps
- Random-Non stationary signals.

- Rough roads
- Cobblestone road

4.3 OpenCRG

OpenCRG is an open source tool-suite for the creation, modification and evaluation of road surfaces. Its objective is to standardize a detailed road surface description. It has applications in tire, vibration and driving simulations where an efficient and reliable road representation is required.

A curved regular grid (CRG) shown in the fig 4.2 represents road elevation data close to an arbitrary road centre line which is defined by consecutive heading angles. The reference line may be complemented by Hilliness (slope, inclination, grade, pitch angle) or Cross Slope (super-elevation, banking, cant, camber, roll angle). Environmental information like friction, temperature, wind velocity and direction can also be handled.

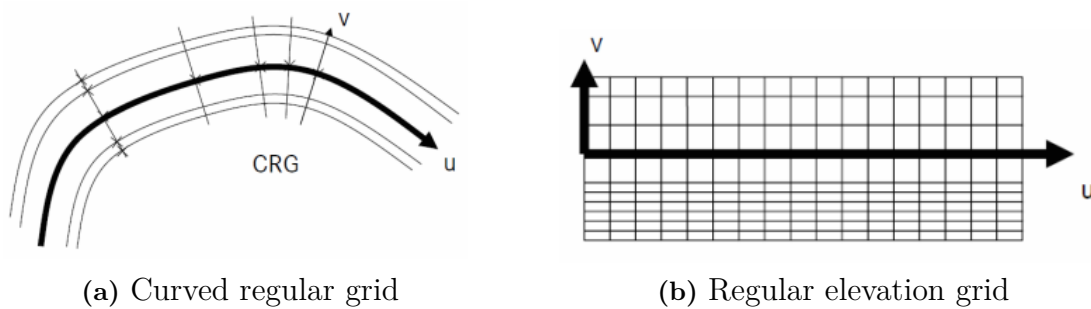


Figure 4.2: Curved regular grid representation [16]

In the figure 4.2a CRG cuts are orthogonal to the reference line and in the figure 4.2b columns and rows are represented by longitudinal and lateral cuts which are orthogonal and parallel to the reference line respectively where data is stored as low precision arrays. Therefore the data is compactly stored reducing the end file size.

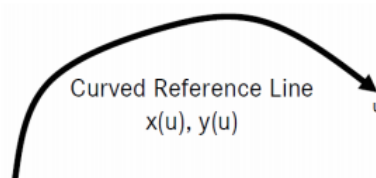


Figure 4.3: Curved reference line [16]

The curved reference line show in figure 4.3 is defined by a high precision start position and low precision heading angles which maintains sufficient accuracy even for long tracks with high altitude. The Potential drift due to path integration is prevented by redundant high precision end location of the reference line. Reference line can also be used as input for steering control/driver models [16].

4.4 Modeling Process

The process of modeling road profiles of both deterministic and random roads can be explained by the following steps. Figure 4.4 also shows the flow of the process.

- *Input:* Input data (such as pothole dimensions and power spectral densities) for modeling virtual proving grounds are obtained through published papers, measured data and ISO standards. This data are imported into Matlab as input to the mathematical and analytical road models.
- *Mathematical and analytical modeling:* The random roads are modelled as stochastic models (section 4.6) to estimate the vehicle fatigue through statistical description and analysis of road surface irregularities.
Deterministic periodic roads are modelled mathematically (section 4.7.2) by defining the road profiles as sinusoidal equations and Non-periodic roads are modelled analytically (section 4.7.1) by representing the events (such as pothole, curb and bumps) as data points along the road profile.
- *Validation:* The stochastic models (such as rough road form class A-H and cobblestone road) are validated using ISO Power spectral densities standards and measured road data. Deterministic models are validated by comparing the modelled road to the input data. Refer section 4.6.3 for validation results.
- *Road profile generation:* The mathematical and analytical models are integrated with OpenCRG (section 4.3) to generate 3D digitized CRG roads used for virtual proving ground simulations using ADAMS/Car. Simultaneously 1D road profile data is stored in an excel file for shaker rig simulations.

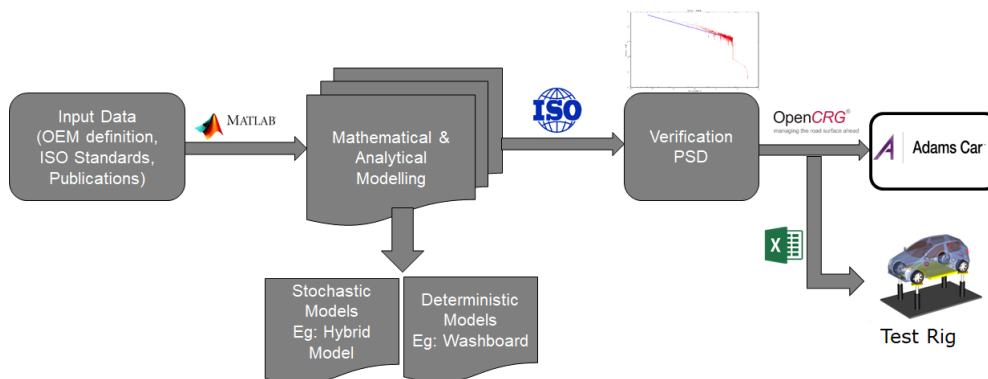


Figure 4.4: Road modeling process

4.5 Road modeling Fundamentals

4.5.1 Power Spectral Density

Power spectral density (PSD) provides information about the distribution of the total power over the entire frequency range. This information can be used to analyze the limiting mean square value of a signal at any frequency. Displacement power spectral density which is the PSD of the vertical road profile displacement is used to analyze the spectrum of the road profiles of the stochastic road models [19,18].

The PSD estimation of infinite number of frequencies, usually that of a auto-correlation function is defined in detail in [19] but in actuality PSD of a finite number of frequencies are estimated using Fast Fourier transforms (*fft*).

The one-dimensional PSD of the road profile is estimated using equation 4.1 by taking *fft* of the vertical road profile displacement and considering only the single sided spectrum. The signal thus obtained is real-valued and has even length. Because the signal is real-valued, you only need power estimates for the positive or negative frequencies. In order to conserve the total power, all frequencies that occur in both the positive and the negative sets are multiplied by a factor of 2 [20].

$$\Phi(z) = \frac{2}{NF_s} \cdot |fft(z(x))|^2 \quad (4.1)$$

4.5.2 Road profile spectrum

The International Organization for Standardization (ISO) uses a one-parameter spectrum (4.2) to define the distribution of power that build a signal. The spectrum (4.2) is obtained by fitting the smoothed measured data by least mean-square method.

$$G_d(\Omega) = G_d(\Omega_0) \cdot \left(\frac{\Omega}{\Omega_0}\right)^{-w} \quad (4.2)$$

Assuming $\Omega_0 = 1 \text{ rad/m}$ and simplifying. We get.

$$G_d(\Omega) = C \cdot \Omega^{-w} \quad (4.3)$$

The roads are classified based on their unevenness measure by the International Organization for Standardization. The roads from high speed highways to extremely rough off-roads are classified from ranges A-H as shown in the figure 4.5 based on their roughness values C and assuming a constant-velocity PSD, which means Waviness parameter $w = 2$ in equation 4.3 where the intensities of all wavelengths of the spectra are equal [21, 22, 18].

$$G_d(\Omega) = C \cdot \Omega^{-2} \quad \Omega \in 2\pi \cdot [0.011, 2.83] \quad (4.4)$$

Spectrum (4.4) is used in the vehicle development process because of its simplicity and it is also used here as a reference measure for the generated rough road models.

However, the road models generated using the spectrum (4.4) does not provide the accurate description of the spectrum for low and high frequency ranges compared to the observed spectrum of the real roads [21].

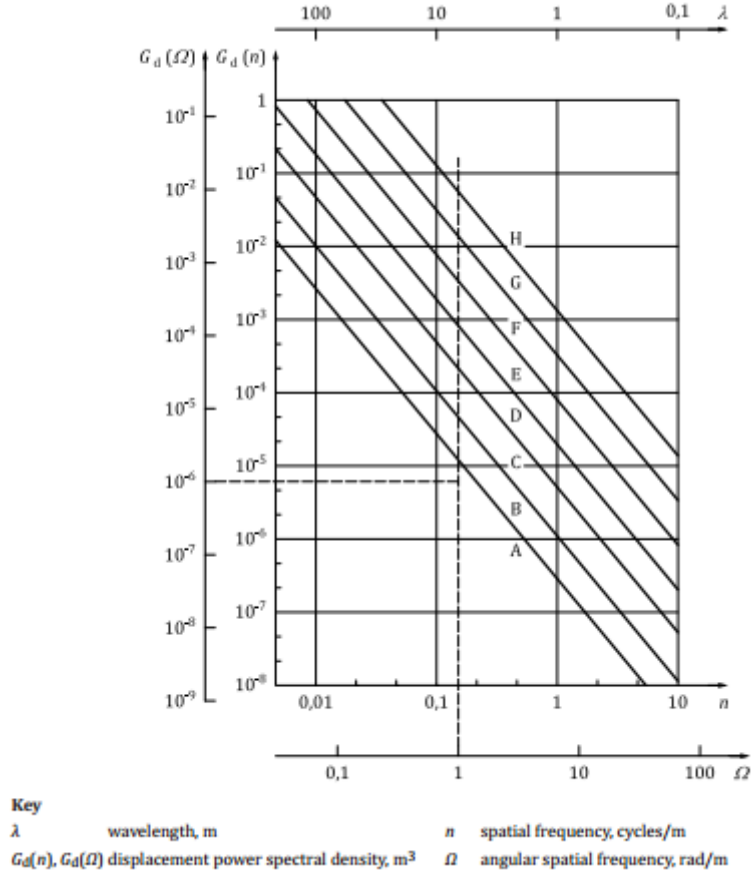


Figure 4.5: ISO classification of roads [18]

Due to the drawbacks of the one-slope spectrum, two-slope spectrum by Motor Industry Research Association (MIRA) is used. There are two version of the MIRA spectrum. The first spectrum (4.5) is mostly used in the modeling of non-homogeneous Gaussian road models. Where, 10^{a_0} is the basic roughness co-efficient, w_1 and w_2 are waviness parameters whose wavelengths lie between $100 - 5 m$ and $5 - 0.1 m$ respectively and $\Omega_0 = 2\pi \cdot 0.2 rad/m$.

$$G_d(\Omega) = \begin{cases} 10^{a_0} \cdot \left(\frac{\Omega}{\Omega_0}\right)^{-w_1} & \Omega \in 2\pi \cdot [0.01, 0.2], \\ 10^{a_0} \cdot \left(\frac{\Omega}{\Omega_0}\right)^{-w_2} & \Omega \in 2\pi \cdot [0.2, 10], \\ 0, & \text{otherwise} \end{cases} \quad (4.5)$$

The second spectrum (4.6) also know as *British standard Institution* (BSI) spectrum is used here to compute Hybrid rough road, Hybrid rough road 3D and Cobblestone road models (section 4.6).

$$G_d(\Omega) = \begin{cases} C \cdot \Omega^{-w_1} & \Omega \in 2\pi \cdot [0.01, 0.2], \\ C \cdot \Omega^{-w_2} & \Omega \in 2\pi \cdot [0.2, 10], \\ 0, & \text{otherwise} \end{cases} \quad (4.6)$$

It should be noted that spectrum's (4.5) and (4.6) does not describe the road roughness spectra for the entire frequency range precisely. But importantly, they give a proper estimation of the energies for the frequencies that excite the vehicle depending on the vehicle velocity [21].

According to Kozubowski et al [23], one can use analytically more track-able Matérn spectra (4.9) with a proper choice of parameters to give a spectra similar to a BSI spectrum (4.5). The Matérn spectra is derived from the Matérn co-variance function (4.7) whose spectral density can be deduced to the general form given by the equation (4.8) [31, 32].

The Matérn class of covariance functions is given by.

$$k_{Matern}(x) = \sigma^2 \cdot \frac{2^{1-v}}{\Gamma(v)} \cdot \left(\sqrt{2v} \cdot \frac{x}{l}\right)^v \cdot K_v\left(\sqrt{2v} \cdot \frac{x}{l}\right) \quad (4.7)$$

where $v, \sigma, l > 0$, are smoothness, magnitude and length scale parameters and K_v is the modified Bessel function.

The spectral density is of the form.

$$G(\Omega) = \frac{Q}{(\lambda^2 + \Omega^2)^{(v+\frac{1}{2})}} \quad (4.8)$$

Where, λ is $\sqrt{2v}/l$.

Modified Matérn spectra is given by.

$$G_d(\Omega) = \frac{C}{\left(c^2 + \left(\frac{\Omega}{\Omega_0}\right)^2\right)^{w_1/2}} + \frac{C}{\left(c^2 + \left(\frac{\Omega}{\Omega_0}\right)^2\right)^{w_2/2}} \quad (4.9)$$

Where, c is a positive constant parameter [21].

4.5.3 Kernel

The PSD of a random process can be represented by many ways. One way is to use a kernel function which captures the similarity of the density function appropriately. Choosing a proper kernel for a given problem is one of the limiting factors of kernel-methods, especially for a non-Gaussian processes.

A simple way to represent a road profile $Z(x)$ [30] is through a convolution of white noise process with kernel function $g(x)$ given by the equation (4.11), which is normalized such that it's square integrates to one and is symmetric, that is,

$g(x) = -g(x)$. Therefore the normalized random process of road profile generation can be generally represented as 4.10.

$$Z(x) = \sqrt{dx} \cdot g(x) * W_i \quad (4.10)$$

$$g(x) = \mathcal{F}^{-1}\left(\sqrt{2\pi \cdot G_d(\Omega)}\right) \quad (4.11)$$

Where, W_i are independent equally distributed random variables with mean zero and variance one, dx is the spatial discretization step and '*' represents the convolution of two vectors. \mathcal{F} in equation 4.11 is the Fourier transform and $G_d(\Omega)$ is the spectrum of choice.

For extensions beyond the Gaussian setup such as Laplace moving average (LMA) process, the co-variance function can no longer uniquely define the distributional and geometric properties of the road profile signal and the shape of the asymmetric kernel defines the shape of the irregularities which control the modal properties. Therefore, estimation of an asymmetric kernel for processes like LMA becomes crucial. A simple construction of an asymmetric kernel given by equation 4.12 can be derived from the Matérn spectra (4.9) [21, 23].

$$\mathcal{F}g(\Omega) = \frac{C \cdot c^{w_1}}{\left(1 + i \cdot L_r\left(c \frac{\Omega}{\Omega_0}\right)\right)^{(2q-1) \cdot w_1/2} \cdot \left(1 + \left(c \frac{\Omega}{\Omega_0}\right)^2\right)^{(1-q) \cdot w_1/2}}, \quad 1/2 < q < 1 \quad (4.12)$$

Where, q defines the symmetricity of the kernel, which gives a symmetric kernel for value $q = 1$, while the value $q = 1/2$ gives a causal one and L_r is the driving direction. We have chosen the asymmetric kernel 4.12 for computing all the stochastic road models, based on the fact that any kernel can be used to define the spectrum of a Gaussian process. This is not the case for LMA process [21], for which a proper kernel should be chosen to uniquely define its spectrum.

4.6 Stochastic road modeling

Stochastic road models are used to describe the variation in measured road profiles and this section focuses on explaining the modeling process of road surface roughness to give an accurate fatigue life estimation of the vehicle components. The models presented here are capable of describing the road surface roughness of very long road sections, with a flexibility to describe the parameters according to the end user.

4.6.1 Rough road modeling

4.6.1.1 Hybrid rough road model

The roads surfaces in practise contains random irregularities such as, potholes and crackles, and most vehicle engineering experts agree that Gaussian distribution does

not accurately represent the actual road surface. Commonly, such processes are often employed to represent an undamaged road surface.

Here we have employed an Hybrid method from Klas Bogsjö et al [21], which is an integration of both stationery Gaussian model and Laplace moving average model. Accurate representations of road surface roughness is accomplished by modeling an undamaged road surface using stationery Gaussian process to which short sections of irregularities and potholes are added by altering the LMA process, resulting in a non-homogeneous, ergodic process.

Stationery Gaussian process

Gaussian process is modelled as a moving average (MA) process, which is a convolution of white noise process Z_i and Matérn kernel function $g(\Omega)$ given by the equation 4.12. The general schema of the Gaussian moving average process is by the equation 4.10 and the kernel $g(\Omega)$ (4.13) is introduced through its Fourier transform $\mathcal{F}g(\Omega)$, which is normalised such that the integral $\int g(\Omega)^2 \cdot dx = 1$.

$$\mathcal{F}g(\Omega) = \begin{cases} \frac{\tilde{c}}{\left(1+i \cdot L_r \left(c \frac{\Omega}{\Omega_0}\right)\right)^{(2q-1) \cdot w_1/2} \cdot \left(1+\left(c \frac{\Omega}{\Omega_0}\right)^2\right)^{(1-q) \cdot w_1/2}}, & \Omega \in 2\pi \cdot [0.01, 0.2], \\ \frac{\tilde{c}}{\left(1+i \cdot L_r \left(c \frac{\Omega}{\Omega_0}\right)\right)^{(2q-1) \cdot w_2/2} \cdot \left(1+\left(c \frac{\Omega}{\Omega_0}\right)^2\right)^{(1-q) \cdot w_2/2}}, & \Omega \in 2\pi \cdot [0.2, 10], \\ 0, & \text{otherwise} \end{cases} \quad (4.13)$$

Where \tilde{c} is a normalized constant and the range of Ω is taken from the BSI spectrum (4.6). Taking the $fft(\mathcal{F}g(\Omega))$, figure 4.6 shows the shape of the Matérn kernel.

Road profile $Z_0(x)$ using GMA is given by.

$$Z_0(x) = \sigma \cdot \sum \sqrt{dx} \cdot \mathcal{F}g(\Omega) * Z_i \quad (4.14)$$

where Z_i 's are zero mean and variance one independent standard Gaussian variables, dx is the discretization step and the fineness of the length of the increment dx defines the smoothness of the kernel, and σ is the variance of the road taken from the BSI or Matérn spectrum [21]. Figure 4.7 shows the undamaged road profile modelled using Gaussian process.

Laplace Moving Average (LMA) model

LMA process is based on a non-homogeneous Laplace model where the road surface models have a generalized Laplace distribution. Non-homogeneous Laplace model is constructed on the idea of non-homogeneous Gaussian model where the road profile $Z(x)$ is assumed to have M equally spaced blocks of length L_0 whose variance is given by R_j . The method to combine this blocks of constant variance to give a smooth

transition between the segments is estimated by MA of Gaussian white noise process.

The non-homogeneous Laplace process to estimate road profiles of each block j is given by

$$Z_j(x) = \sum_{(j-1)L_0 < x_i \leq jL_0} \sqrt{dx} \cdot \sqrt{R_j} \cdot g(x - x_i) * Z_i \quad (4.15)$$

Where, R_j is the variance given by independent gamma-distributed random variables having shape parameter $1/\nu$ and scale ν .

Road profile $Z(x)$ is given by

$$Z(x) = \sum_{j=1}^M Z_j(x) \quad (4.16)$$

The LMA can be illustrated as a series of impulses due to the net accumulation of jump values of the Laplace motion. It is given as the limit to the non-homogeneous Laplace process as $L_0 = dx$ and $\sqrt{(dx \cdot R_j)}$ is substitute with $\sqrt{\Gamma_j}$, so that variance $V[Z_j \sqrt{\Gamma_j}] = dx$.

The jump process of LMA is given by.

$$Z_{Lma}(x) = \int g(x - u) d\Lambda(u) = \sigma \cdot \mathcal{F}g(\Omega) \sum_{i=1}^N Z_i(x) \quad (4.17)$$

$$Z_i(x) = \sqrt{\nu} \cdot \sqrt{(e^{\nu\gamma_i/L})} \cdot \sqrt{W_i} \cdot U_i \quad (4.18)$$

The Z_i 's normalized such that it has zero mean and variance one. Where W_i are independent and identically distributed standard exponential variables independent of γ_i and U_i , and γ_i is the location of the i th point in a Poisson process, that is, $\gamma_i = \sum_{j=1}^i G_j$, where G_j are independent standard exponentially distributed random variables. Finally, U_i are independent random variables distributed uniformly on $[0, L]$.

And the parameters ν and N are given by.

$$\nu = \hat{\nu} = \frac{\hat{k}_e}{3 \int \mathcal{F}g(\Omega)^4 dx} \quad (4.19)$$

$$N \approx -2 \cdot \frac{L}{\nu} \cdot \ln(p) \quad (4.20)$$

Where $\sqrt{\Gamma_j}$ are independent gamma-distributed variables having shape parameter dx/ν and the scale equal to ν . ν is the shape parameter in Laplace motion $\Lambda(x)$. \hat{k}_e is the excess kurtosis ($k_e > 3$) that controls the tailedness and sharpness of the irregularities. And, N represents the number of irregularities which is controlled by the irregularity parameter p [21]. Figure 4.7 shows the irregularities modelled by

the LMA process.

Hybrid Model

The road profile $Z(x)$ can now be defined by the Hybrid process as.

$$Z(x) = pZ_0(x) + Z_{Lma}(x) \quad (4.21)$$

Simplified as,

$$Z(x) = \sigma \left(\left(p\sqrt{dx} \sum_{i=1}^{N_n} Z_i + \sum_{i=1}^N Z_i(x) \right) * \mathcal{F}g(\Omega) \right) \quad (4.22)$$

Where $Z_0(x)$ and $Z_i(x)$ in equation 4.21 are taken from the equations 4.14 and 4.17 respectively and N_n is given by L/dx . Figure 4.7 shows the road profile $Z(x)$ modelled using the Hybrid process.

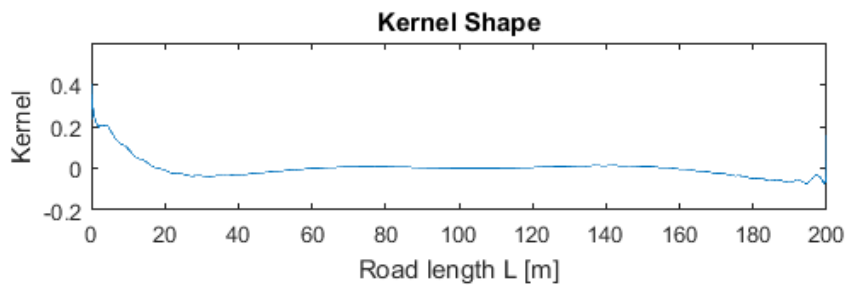


Figure 4.6: Shape of the kernel function 4.13

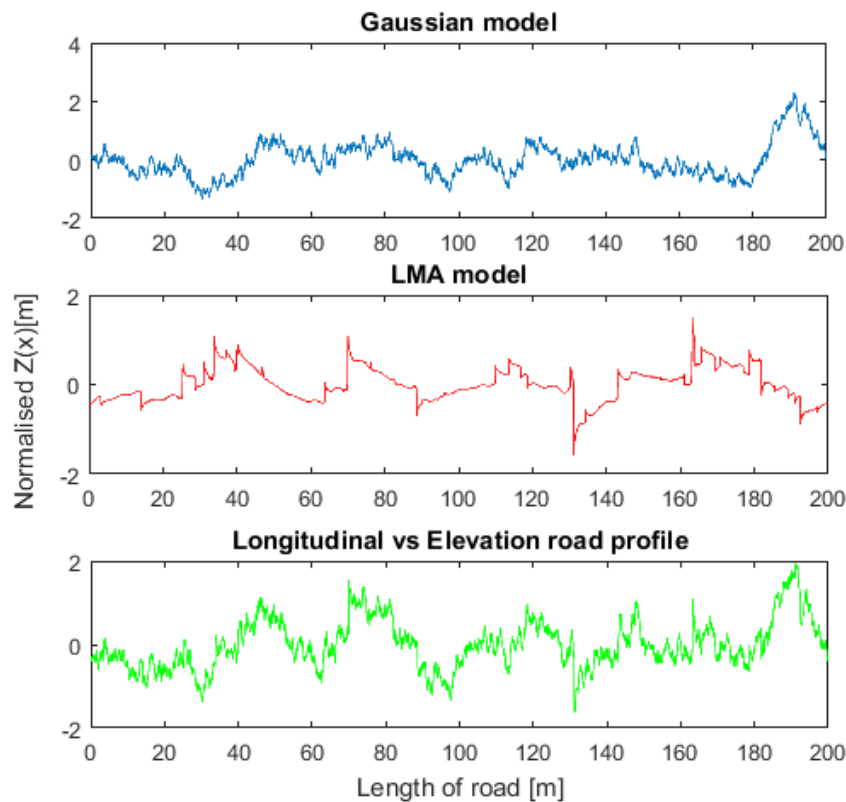


Figure 4.7: Hybrid Process: Top- Normalized Gaussian model; Middle- LMA model; Bottom- Combined Hybrid model

The irregularities modelled by LMA process takes the shape of the kernel function 4.13 which can be observed from the figures 4.7 and 4.6. The locations of the irregularities are distributed randomly over the road length L and have random amplitudes. The irregularities contains both the long wave and short wave components in the range of frequencies of the spectrum 4.6. The hybrid model with $p = 1$ becomes a Gaussian model which underestimates the fatigue damage and with $p = 0$ it represents a LMA jump process which tends to overestimate the fatigue damage. Hybrid model with p between the two extremes can give a reliable damage estimation, moreover the value p can be adjusted to give an accurate estimation of damage granted a reference index is available [21].

Table 4.1 and 4.2 shows the parameter and roughness values used in the the hybrid road model.

Table 4.1: Hybrid model parameters

Parameter	Value used	Possible range
Ω_0 [rad/m]	1	-
dx [m]	10^{-2}	$10^{-1} - 10^{-3}$
w_1	2.6	-
w_2	2.1	-
k_e	3.1	3.1 – 9
p	0.6	0 – 1
q	0.7	0.5 – 1
L_r	-1	-1 or 1
\tilde{c}	10	-

Table 4.2: ISO degree of roughness [18]

Degree of Roughness	
ISO Road class	$C(\Omega)$ [$10^{-6}m^3$] Mean
A	1
B	4
C	16
D	64
E	256
F	1024
G	4096
H	16384

4.6.1.2 Hybrid multi-variate rough road model

Taking the idea from the Hybrid model which is essentially an uni-variate road model i.e. the road surface roughness does not vary along the lateral direction (Y) of the road, we have modelled a multi-variate road model whose road surface roughness vary both in the longitudinal (X) and lateral directions (Y) of the road.

The surface roughness of the real roads primarily varies longitudinally and the variations along the lateral road section even though in comparison are small should be modelled for accurate estimation of fatigue damage index. Here it is modelled as two individual layers, a primary uni-variate layer having roughness $C_m = C - C_0$ and a secondary multi-variate non-homogeneous disturbance layer having roughness C_0 . Here C_0 given in the table 5.1 is a lot smaller than the corresponding C value in table 4.2. This secondary layer is meshed on top of the primary layer to give a multi-variate hybrid model.

The modeling process is given by the following steps.

1. A road elevation profile $Z(x)$ of size $N_u \times 1$ is generated using the Hybrid process (4.6.1.1) with $w_1 = 2.9$ and $w_2 = 2.3$ and the other parameters and new roughness values C_m according to the tables 4.1 and 5.1 respectively.
2. Uni-variate 3D road elevation matrix of size $N_u \times N_v$ is computed by replicating the values of the row matrix $Z(x)$ over N_v columns as shown in the figure 4.8.

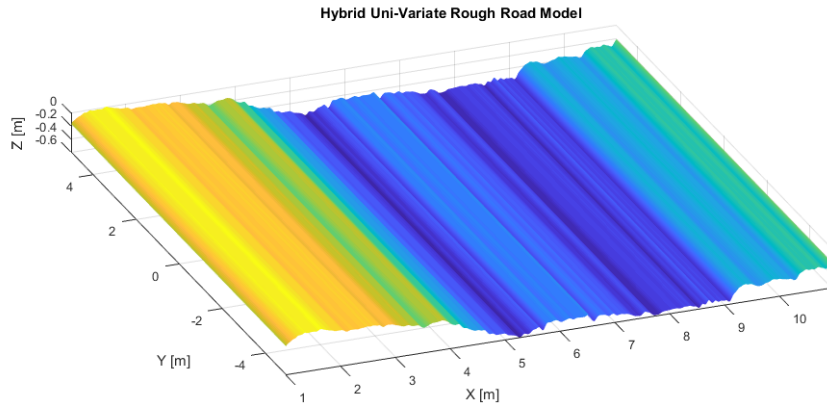


Figure 4.8: Hybrid uni-variate model (Road class C)

3. Multi-variate 3D road elevation matrix is computed by simulating the Hybrid process N_v times to generate a 3D mesh of size $N_u \times N_v$ as shown in the figure 4.9. But here Roughness value C_0 are taken from the table 5.1.

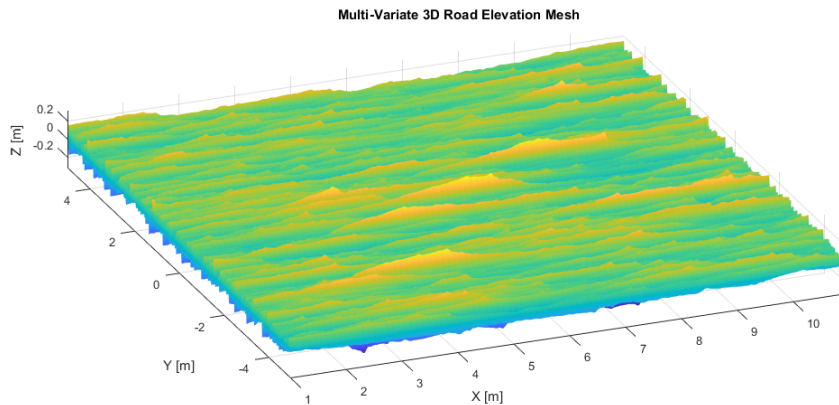


Figure 4.9: Multi-variate 3D road elevation mesh

4. Hybrid multi-variate rough road model as shown in the figure 4.10 is generated by merging the uni-variate elevation elevation matrix with the multi-variate elevation mesh from steps 2 and 3.

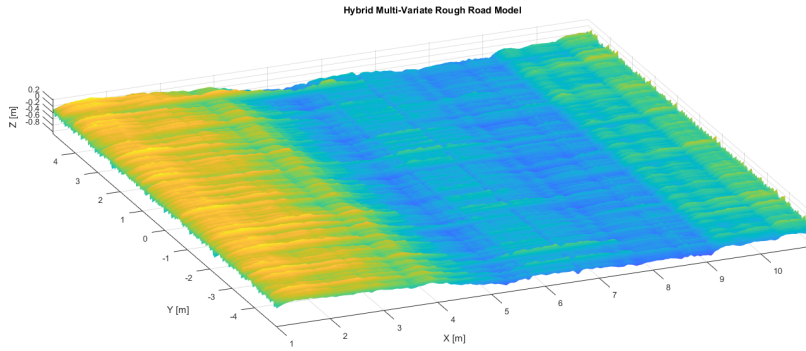


Figure 4.10: Hybrid multi-variate model (Road class 3)

Table 4.3: Modified ISO roughness values

Degree of Roughness		
ISO Road class	$C_m(\Omega) [10^{-6}m^3]$	$C_0(\Omega) [10^{-6}m^3]$
A	0.875	0.125
B	3.5	0.5
C	14	2
D	60	4
E	240	16
F	960	64
G	3842	256
H	15360	1024

4.6.2 Belgian road modeling

Generally virtual models of Cobblestone road a.k.a. Belgian road are usually generated using data from laser scanning and profilograph techniques. This methods are expensive, time consuming and requires pre-processing of raw data. Here we describe a novel method to generate a detailed virtual digitized Belgian road by considering the shapes and sizes of the actual cobblestone blocks, thereby also preserving the shape of the actual Belgian road.

The road profile elevations (Z) of the model presented here vary both in the longitudinal (X) and lateral (Y) directions. The modeling aspect also considers the surface roughness along with different shapes and sizes of the cobblestone blocks. The spaces between the neighboring blocks both in longitudinal and lateral directions are also modelled. To achieve a longitudinally and laterally varying elevation profile, the heights of the Cobblestone blocks are computed by a combined uni-variate 3D road model and interpolated lateral road profile model, both generated via the Hybrid process (4.6.1.1).

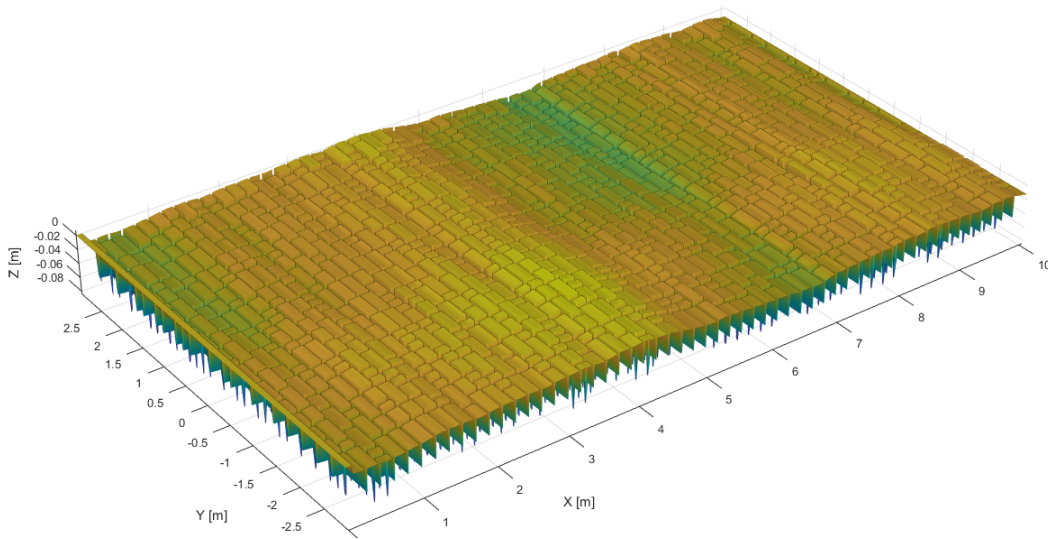


Figure 4.11: Belgian road model

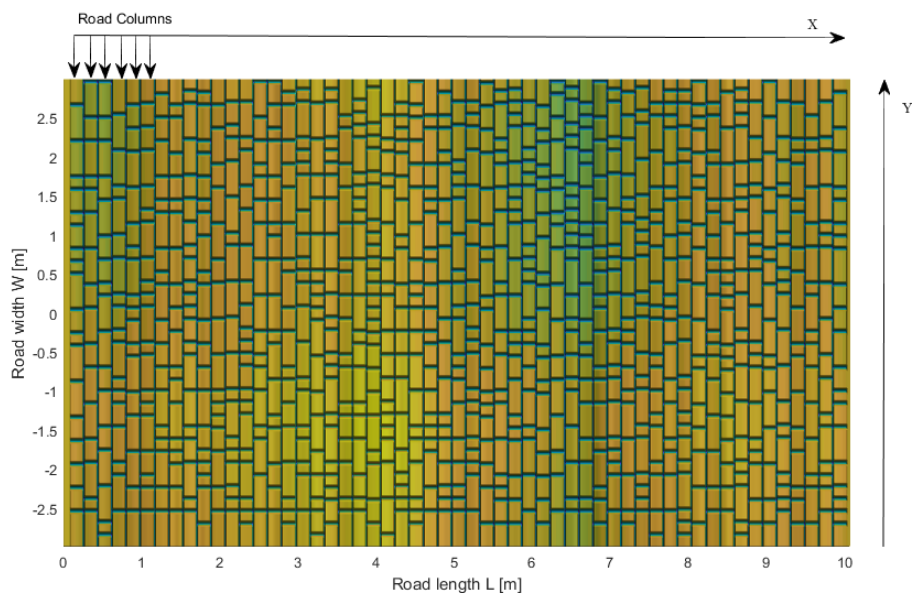


Figure 4.12: Belgian road top view

The methodology of modeling the Belgian road is described by the following steps.

1. **Longitudinal road profile $Z(X)$:** A uni-variate 3D road model of road class C is generated using the Hybrid process with parameters according to table 4.4.
2. **Computing cobblestone block:** Hexagonal blocks with surface roughness as shown in the figure 4.13 are formed by dividing the road created in step 1 into small finite cells of varying sizes, with each cell representing a single block according to the dimensions specified in the table 4.4. Each cell is a matrix of size $(n_r \times n_c)$ containing road elevation data. As shown in the figure 4.13, the length of n_r varies randomly according to width (W_c) of a block and the

4. Road Profile modeling

length of n_c is constant as all the blocks have the same length (L_c). Finally, the spaces in terms of width (w_s) and depth (d_s) between each adjacent cells are created.

$$n_r = W_c/dx ; \quad n_c = L_c/dx \quad (4.23)$$

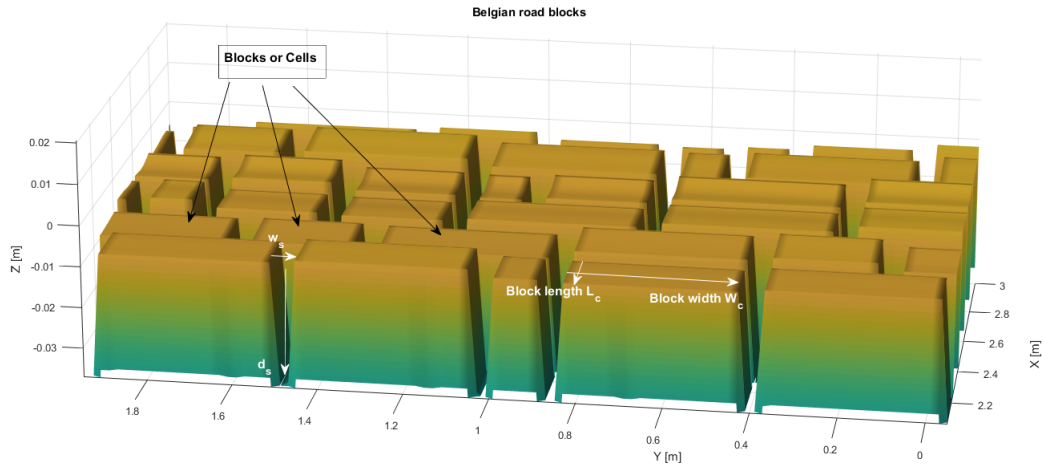


Figure 4.13: Hexagonal Belgian blocks

- Lateral road profile $Z(Y)$:** To create a road profile varying in the lateral direction the height of each cell block is shifted. This is realized by generating a lateral road profile using the Hybrid process (parameters: table 4.4) for the length equal to the width of the road. The generated road profile is then interpolated to the length of the number of cells N_{Cn} in column Cn of the road, where N_{Cn} varies randomly for each column. The interpolated road profile data which are essentially heights are added to each corresponding cell in a column to define the lateral profile as shown in figure 4.14. This process is repeated for rest of the columns of the road to get the final Belgian road model as shown in the figure 4.12 and 4.11.

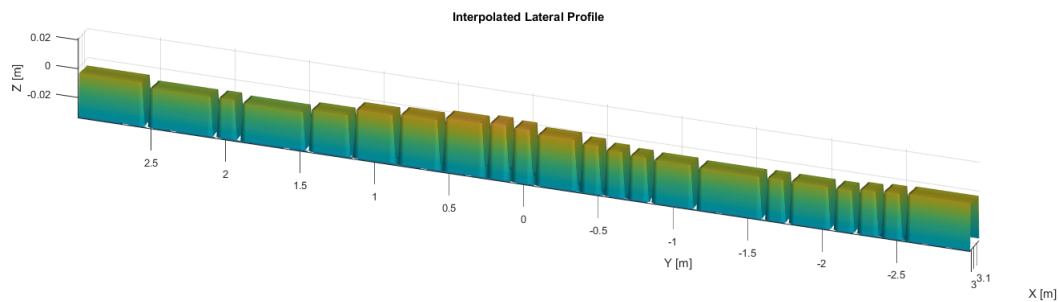


Figure 4.14: Belgian road lateral profile

4.6.3 Validation of Road Models

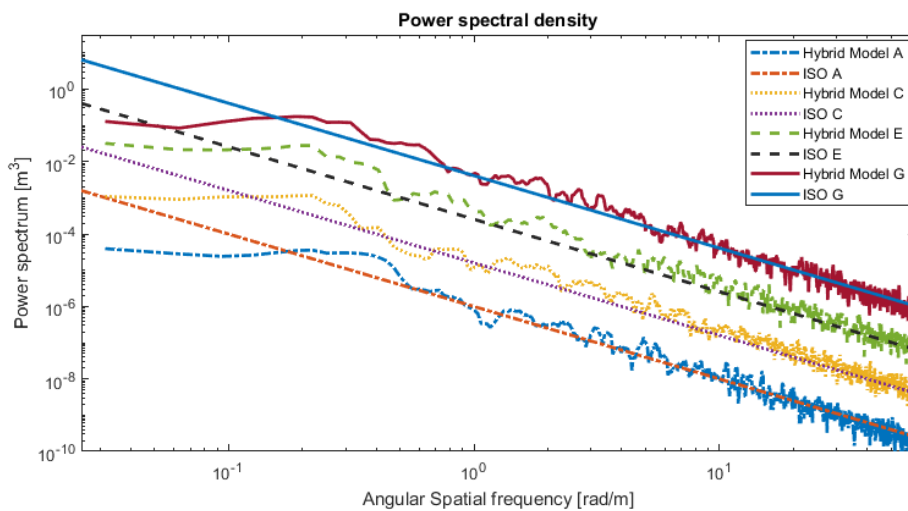
Power spectral density can be defined in several ways and this makes it difficult to compare published data without knowing how the power spectral density has been

Table 4.4: Belgian road model parameters

Model parameters			Belgian road dimensions	
Parameters	$Z(X)$	$Z(Y)$	Dimension [m]	Value
$C(\Omega)[10^{-6}m^3]$	16	4	Length L_c	0.18
$\Omega_0[\text{rad/m}]$	1	1	Width W_c	0.07, 0.15, 0.22
$dx[\text{m}]$	10^{-2}	10^{-2}	Gap length l_s	0.02
w_1	1.5	1.5	Gap width w_s	0.02
w_2	3	3	Gap Depth d_s	0.04
k_e	3.1	3.1	Road width W	3
p	0.8	0.8	Road length L	50
q	0.7	0.7		
L_r	-1	-1		
\tilde{c}	10	10		

defined. Here we are using displacement PSD given by the equation 4.4 defined in ISO:8608 (18) as a standard for comparison. The PSD of the modelled roads are estimated using the equation 4.1 and are one-dimensional in nature. The PSD's are plotted using a logarithmic scale to have an easy understanding of the spread of energies for all the frequencies.

The PSD's of the uni-variate Hybrid road model for the road classes $A - H$ are shown in the figure 4.15 and 4.16.

**Figure 4.15:** PSD of Hybrid uni-variate road model (Road class A, C, E, G)

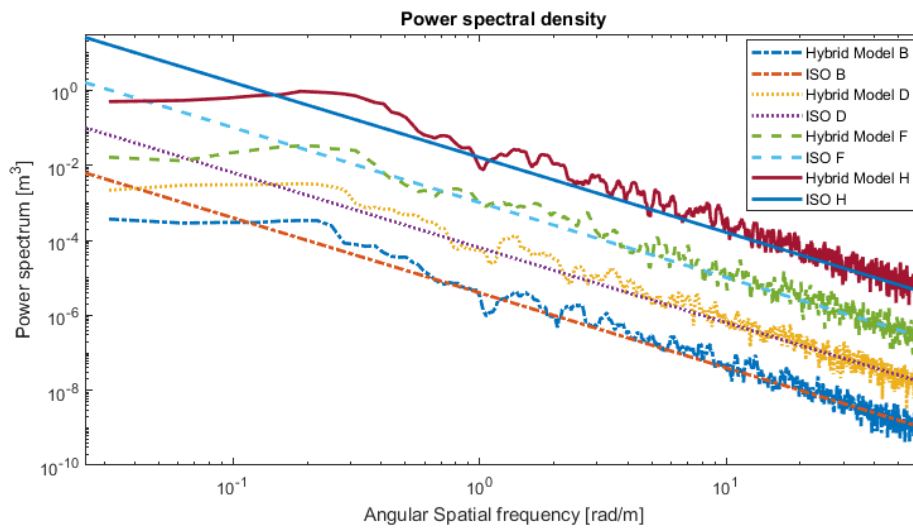


Figure 4.16: PSD of Hybrid uni-variate road model (Road class B, D, F, H)

The PSD's of the multi-variate Hybrid road model for the road classes *A* – *H* are shown in the figure 4.17 and 4.18.

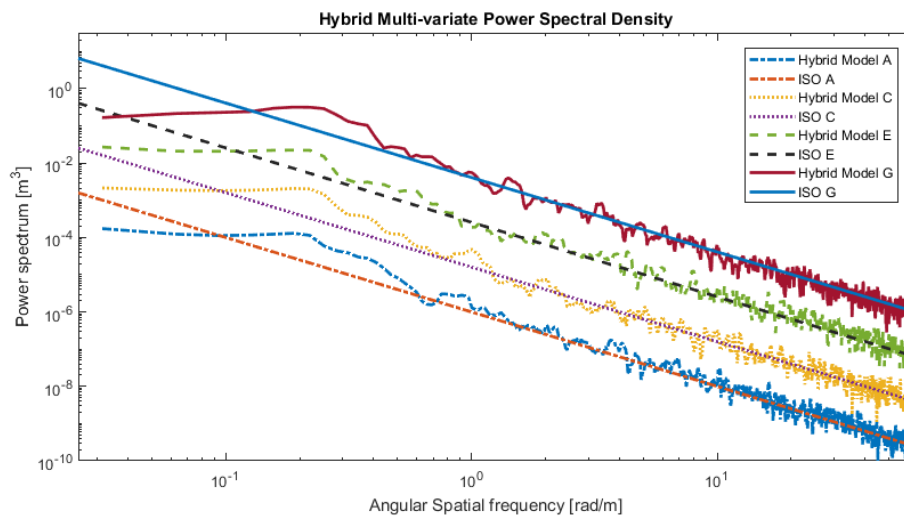


Figure 4.17: PSD of Hybrid multi-variate road model (Road class A, C, E, G)

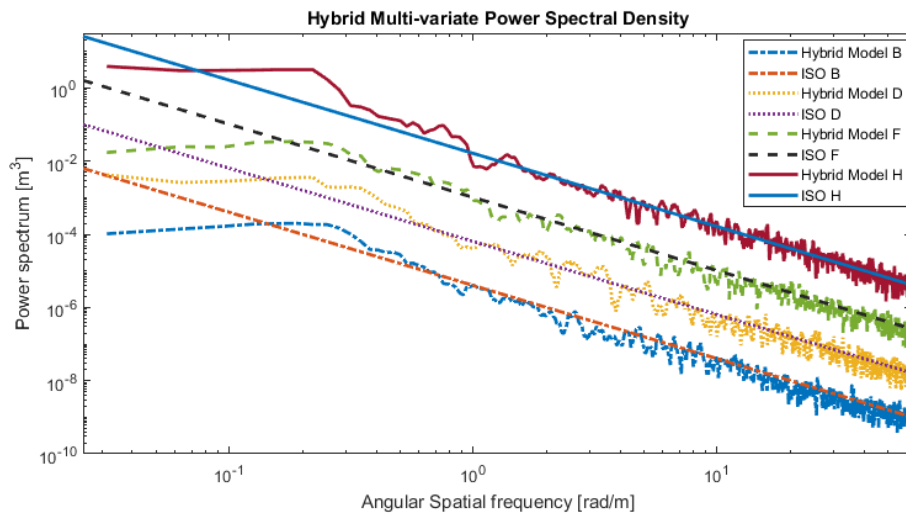


Figure 4.18: PSD of Hybrid multi-variate road model (Road class B, D, F, H)

There is no defined classification of PSD for Belgian roads. Their PSD's are comparable to the ISO road classes and have a unique characteristic nature of repeating orders as shown in the figure 4.19. This are caused by the repetitiveness of blocks length and gaps between adjacent blocks. The PSD's of the cobblestone road model for the road class *C* is shown in the figure 4.19.

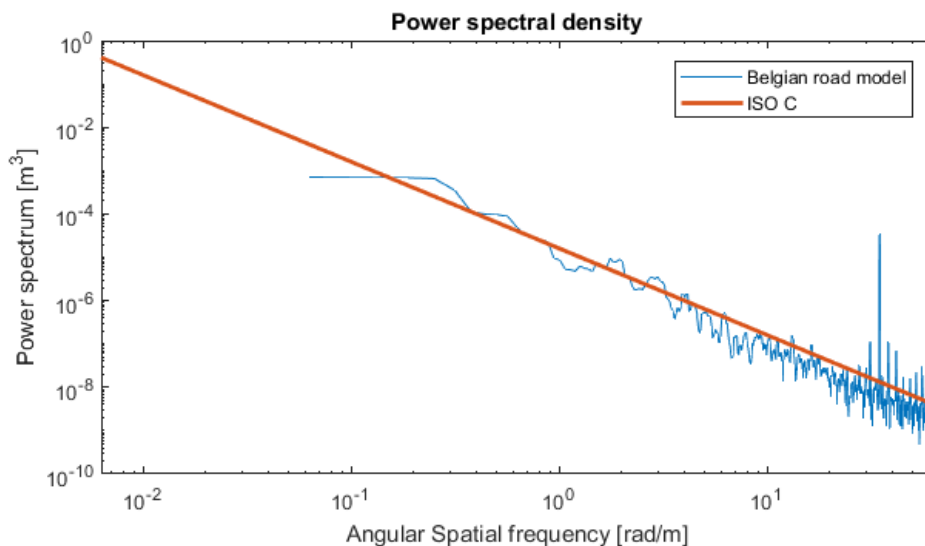


Figure 4.19: PSD of Belgian road model (Road class C)

4.7 Deterministic Road modeling

Deterministic road models are simple models used to define single-event obstacles or repeating periodic road profiles.

4.7.1 Pothole, Curb and Bumps

This are non-periodic single-event obstacles whose elevations road profile $Z(X, Y)$ are represented as series of data points along the longitudinal X and lateral Y road profiles.

The elevation road profile of the roads with potholes and curbs shown in figure 4.20c and 4.20a can be given by a square wave or series of square waves whose elevations are equal to the depth and height of the pothole and curb respectively given by the equation 4.25. The elevation matrix for a pot hole and curb is of the size $(N_L \times N_W)$ where N_L and N_W are number of data points along X and Y respectively and is given by the equation.

$$N_L = L/dx ; \quad N_W = W/dx \quad (4.24)$$

$$Z_{N_L \times N_W} = H \quad (4.25)$$

Trapezoidal bumps as shown in the figure 4.20b are modelled similarly to a curb, except the sides are angled.

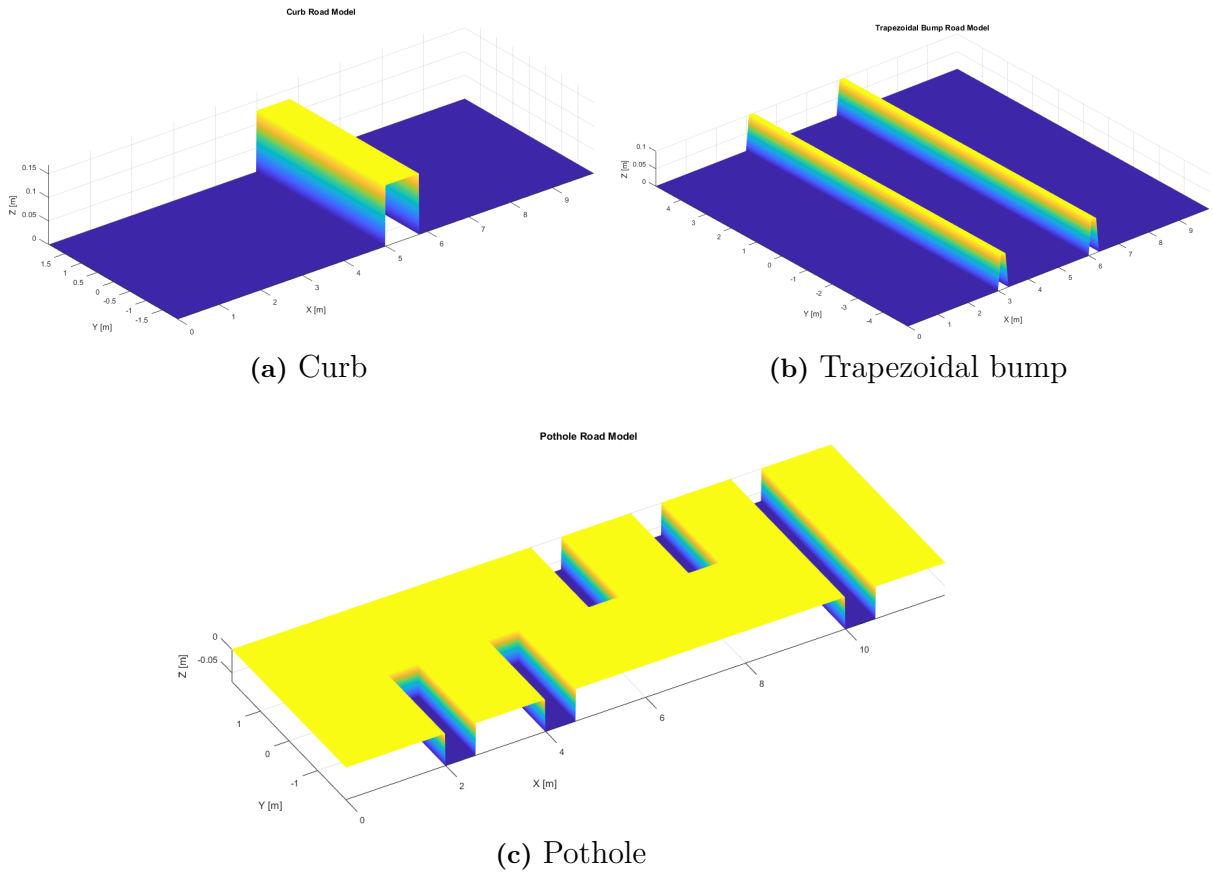


Figure 4.20: Non-periodic road models

4.7.2 Washboard

Washboard is a periodic sinusoidal road with sin forms both in phase and out of phase on LHS and RHS of the road as shown in the figure 4.21.

The elevation road profile $Z(x)$ is given by sin wave equation 4.26. For in phase washboard road the elevation profile $Z(x)$ of size $(N_u \times 1)$ is replicated over the entire road width of size $(1 \times N_v)$. For out of phase washboard road $Z(x)$ with phase difference $\phi = \pi/2$ is generated, the first half width of the road is replicated with $Z(x)$; $\phi = 0$ and other half with $Z(x)$; $\phi = \pi/2$.

$$Z(x) = A \cdot \sin(2\pi f x + \phi) \quad (4.26)$$

Where A is amplitude of the sin wave, f is spacial frequency, x is longitudinal abscissa variable and ϕ is phase difference.

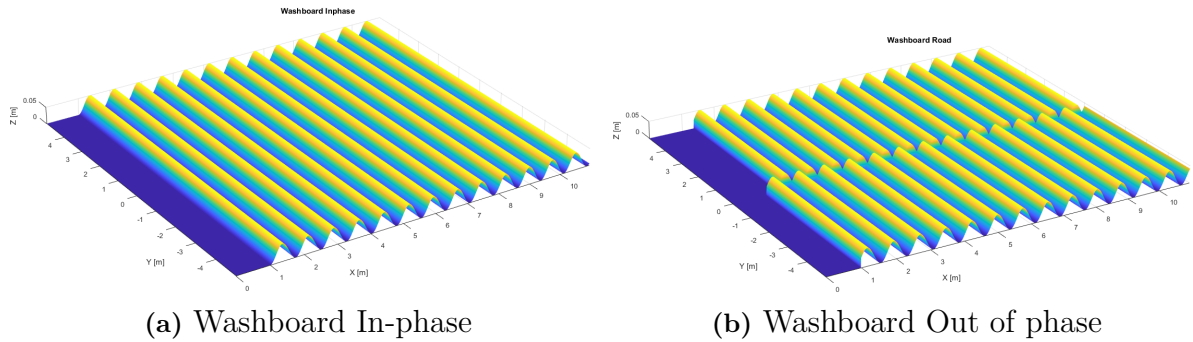


Figure 4.21: Periodic road models

5

Results

This section discusses the results obtained from the simulation using the methodology discussed in the previous chapters.

5.1 Modal Analysis of Body-in-White (BiW)

The BiW of the vehicle was simulated for the same range of frequency of 0-33KHz by appropriately choosing the number of modes to be solved. The effect of the presence and absence of the vehicle masses and windshields in BiW were investigated on the number of modes and their corresponding natural frequencies.

It is found that the BiW *without* the mass and the windshields has lower frequency magnitude for a given mode number compared to the BiW *with* mass and windshields. This trend continues as the mode number increases. In other words, a given value of frequency moves down the scale of mode numbers as the mass and windshields are added to the vehicle body. This is shown in the below figures (Figure 5.1 and Figure 5.2). Additionally, it is observed that as the masses are added the total number of modes for the structure decreases. For example, the BiW *without* the mass and the windshields has 139 modes and the BiW *with* mass and windshields has 133 modes in the frequency range of 0-150Hz. This is because, when the windshields and masses are added, it makes the structure more stiffer.

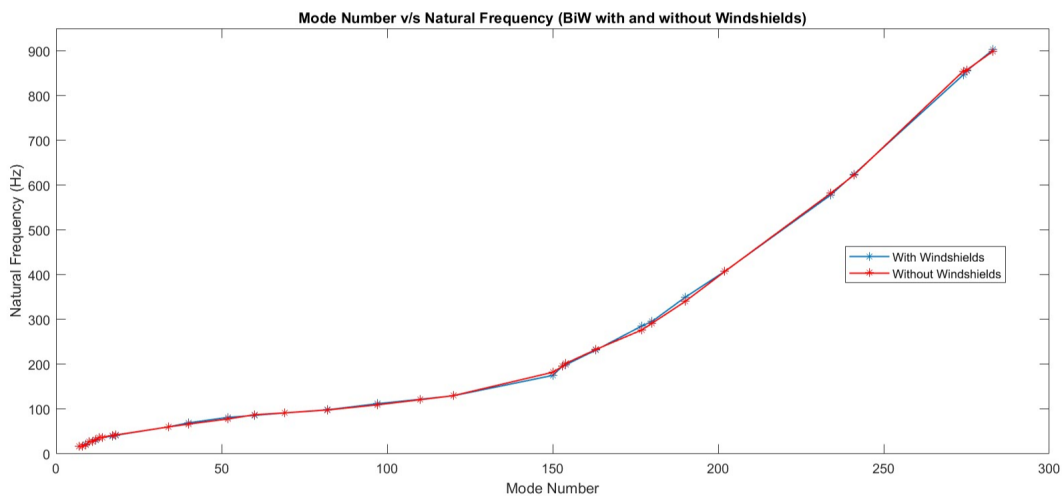


Figure 5.1: Modal Analysis With and Without windshields

5. Results

The modal frequencies obtained by simulating in NASTRAN were compared with the experimental frequencies obtained from [14] for a BiW without windshields and masses. The experimental procedure is explained more in detail in [14] [13]. Although, it was for a similar type but a different vehicle, it was found that the global modes correlate as shown in the table (Table 5.2).

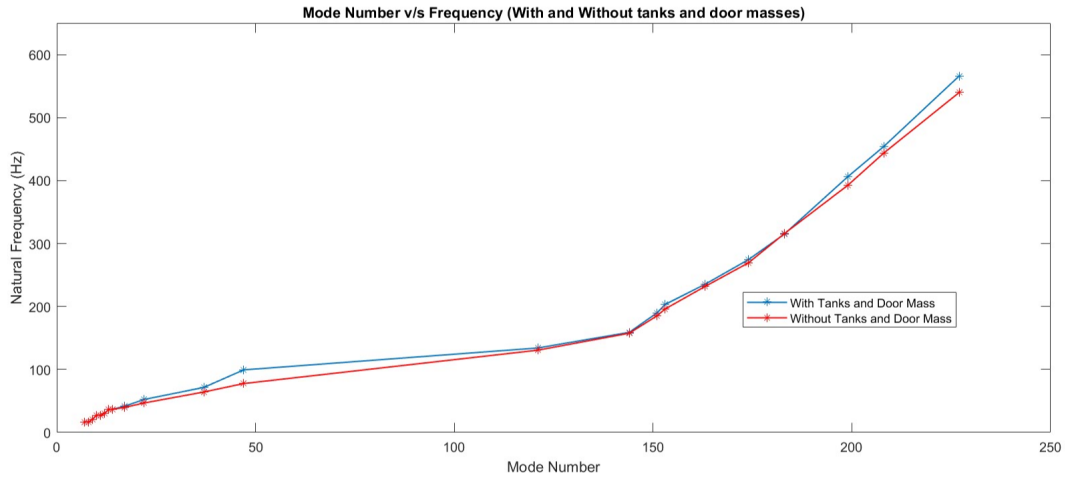


Figure 5.2: Modal Analysis With and Without Masses

Table 5.1: Experimental and Theoretical Modal Analysis Without windshields

Mode Number	Simulated Natural Frequency (Hz)	Tested Natural Frequency (Hz)
1	30	27.50
2	39	31.12
3	44	39.24
4	45	44.33
5	51	51.56
6	53	55.14
7	66	58.21

5.2 Dynamic Simulations for Stress Calculations

The simulation results of the two tire models viz., Pac2002 (With belt dynamics) and UA-Tire are compared with FTire to check the validity of this tire models in durability simulation. Here we perform Pearson correlation [39] of the normal forces to determine the correlation coefficients r , which gives a measure of linear dependency between the models. The range of values for the correlation coefficient is -1 to 1. -1 representing a direct negative correlation, 0 representing no correlation, and 1 representing a direct positive correlation.

5.2.1 Curb Impact Load case

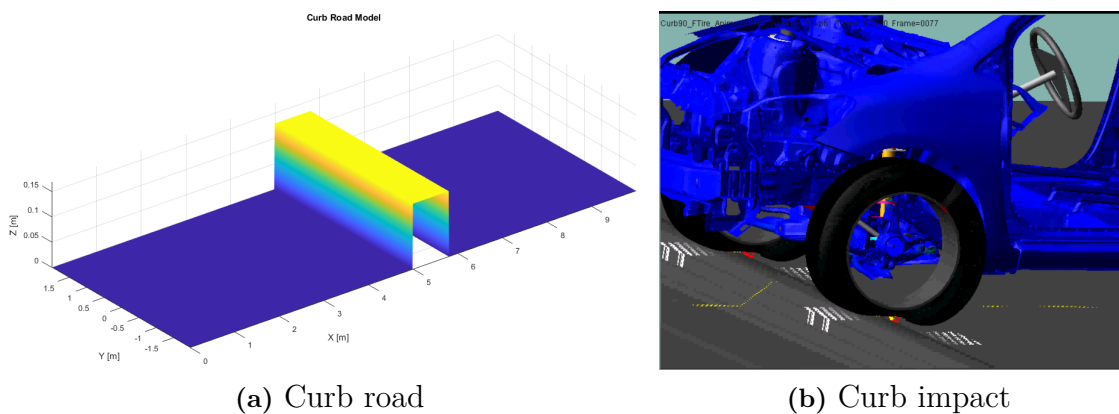


Figure 5.3: The vehicle going over a road with a curb

The car model was driven over a road with a curb of 90mm in height with three different tire models viz., FTire, Pac2002 (With belt dynamics), and UA-Tire at a speed of 50 km/h . The normal force F_Z on the front left tires with respect to time is shown in figure (Figure 5.4) and the FFT of the normal forces is shown in the figure 5.5.

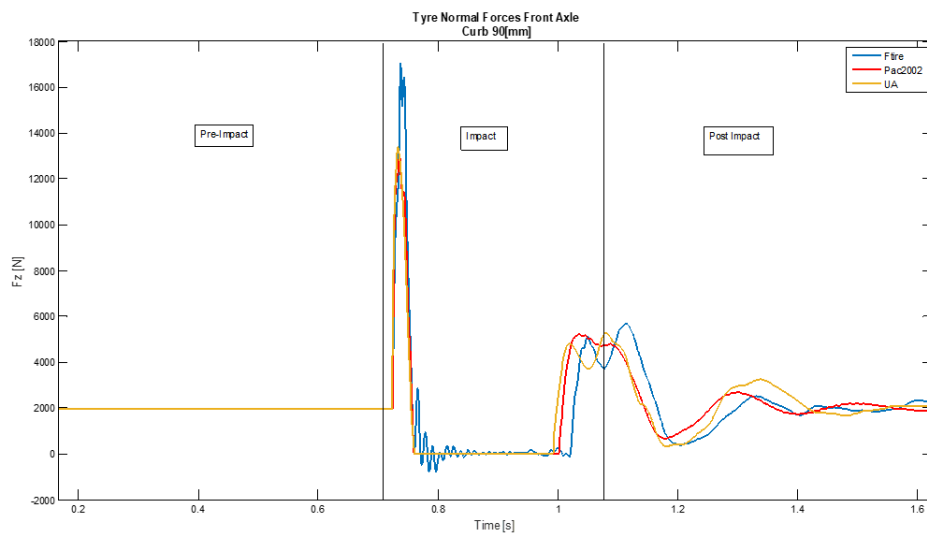


Figure 5.4: Normal Force on the Left Front Tires

From the figure 5.4 it can be observed that during the impact the front tire loses contact with the ground and the normal forces of the corresponding tires of both Pac2002 and UA tire models have zero forces. This is because the deflection ρ and the deflection rate $\dot{\rho}$ in the equations 3.2 and 3.3 are zero as the road height and road plane information from the 3D enveloping model is unavailable. But FTire still exhibits some forces even after losing contact with the road as a result of internal structural stiffness and damping of FTire, calculated using modal data [33].

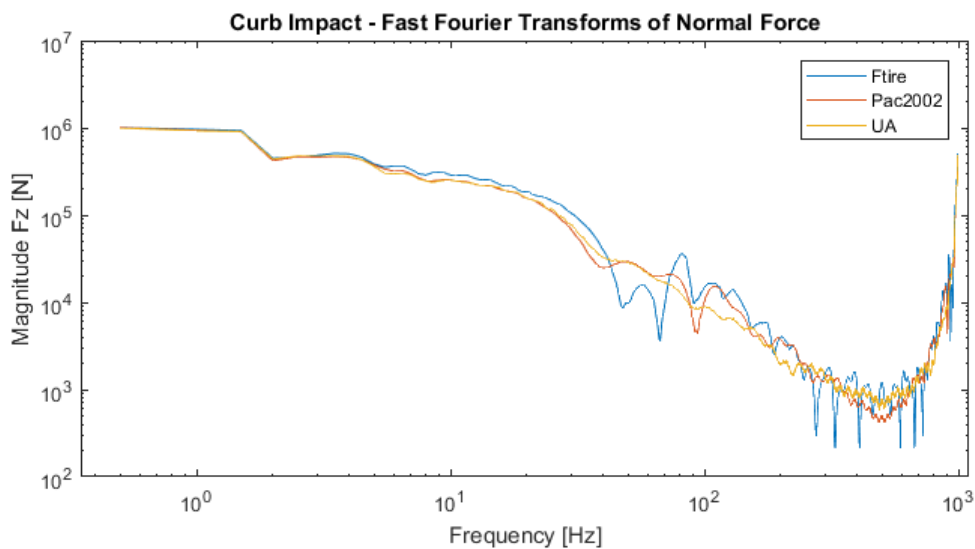


Figure 5.5: Fast Fourier Transform of the normal forces (Curb Impact)

It can also be observed from the figure 5.5 that the FTire model is more accurate in capturing the peak forces at a high frequency range of 80Hz-200Hz compared to Pac2002 and UA-Tire model. It can also be seen that Pac2002 has a fairly better correlation with FTire compared to UA tire model below 250 Hz frequency range. And comparing the correlation of the normal force signals of Pac2002 and UA-Tire

models with the FTire. It is found that Pac2002 has a very high correlation of $r_{Pac} = 0.902$ and UA-Tire model has a moderate correlation of $r_{UA} = 0.863$ with the FTire model respectively. From this we can conclude that in the absence of FTire license, Pac2002 with belt dynamics is still a viable option for simulations with curb impact compared to other ADAMS/Car tire models.

5.2.2 Pothole Load Case

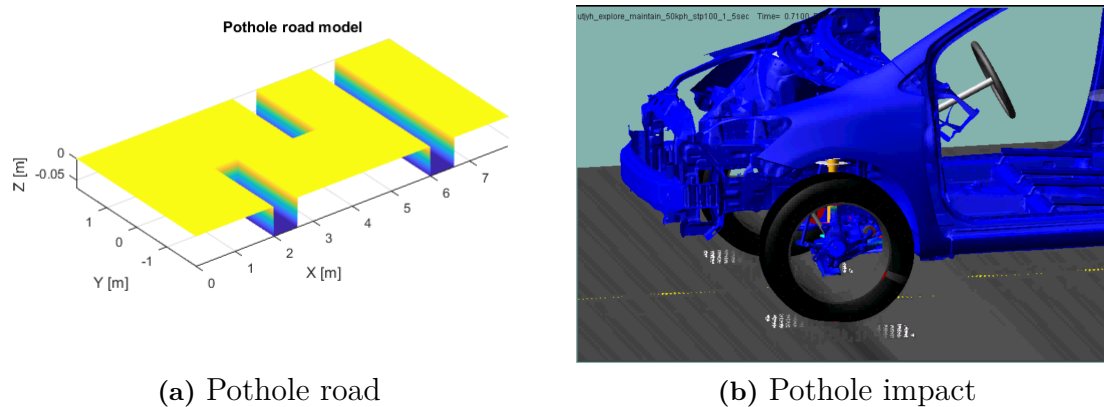


Figure 5.6: The vehicle going over a road with potholes

The ADAMS/Car vehicle model was simulated on a road with three potholes of depth 70 mm and length 60.96 mm as shown in the figure 5.9a with three different tire models viz., FTire, Pac2002 (With belt dynamics), and UA-Tire at a speed of 50 km/h . The normal force F_Z on the front left tires with respect to time is shown in figure 5.7 and the FFT of the normal forces is shown in the figure 5.8.

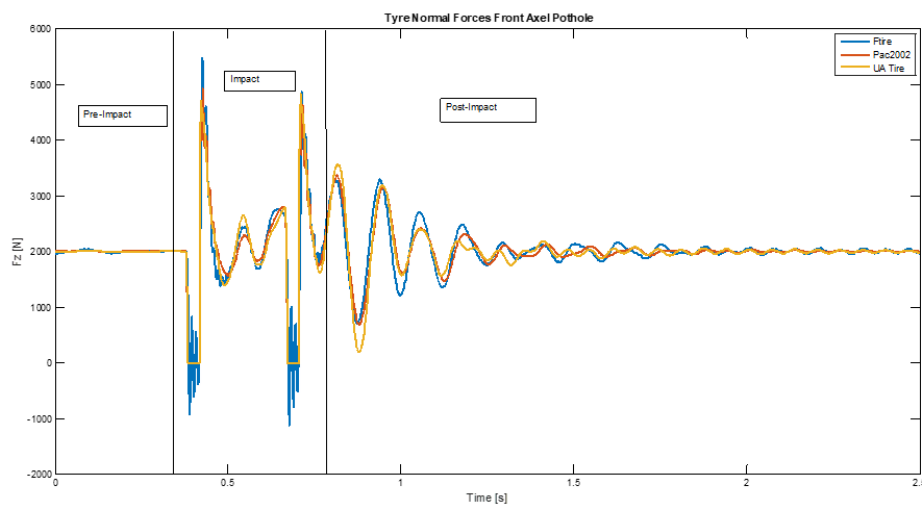


Figure 5.7: Normal Force on the Left Front Tires

Similar to the curb impact, the impact zone of the figure 5.7 shows the normal force of Pac2002 and UA tire models are momentarily zero as the front wheel goes over the pothole without contacting the bottom surface and hits the leading edge of the pothole, giving rise to the peak forces. While the normal force of FTire does not become zero as the tire remains excited due to the internal structural stiffness and damping of the tire.

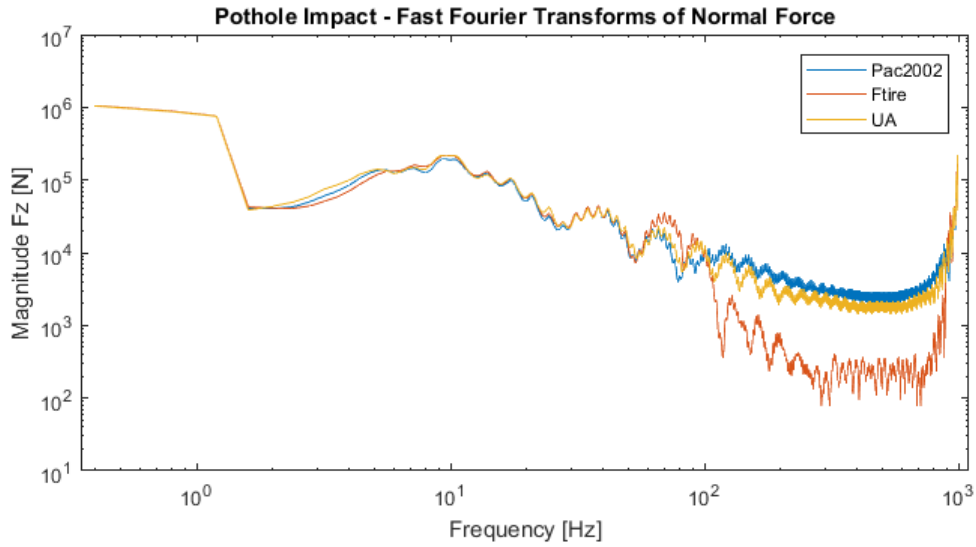


Figure 5.8: Fast Fourier Transform of the normal forces (Pothole Impact)

From the figure 5.8 it can be observed that the Pac2002 and UA tire models only correlate with the FTire up to the frequency of 100 Hz. Above 100 Hz both Pac2002 and UA over estimate the normal forces resulting in over estimation of damage on the components. Comparing the correlation coefficients of the normal force signals of Pac2002 and UA tire models with the FTire. We find that Pac2002 has a high correlation of $r_{Pac} = 0.935$ and UA has slightly lower correlation of $r_{UA} = 0.916$ than Pac2002. It can also be observed in the response zone of the figure 5.7 that Pac2002 has a better correlation with FTire compared to UA tire model. Therefore Pac2002 with belt dynamics can be used in the absence of FTire for Pothole simulation to get satisfactory results.

5.2.3 Rough Road Load Case

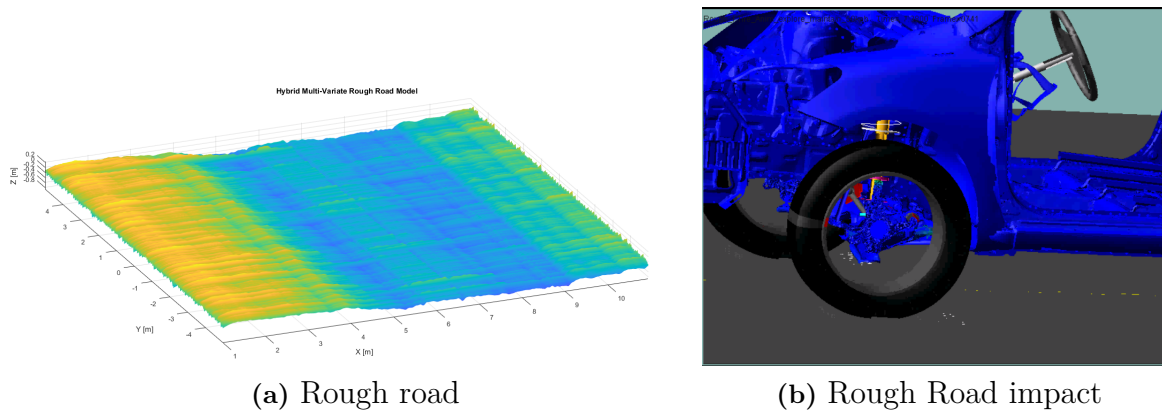


Figure 5.9: The vehicle going over a rough road

The ADAMS/Car vehicle model was simulated over a hybrid multi-variate rough road of road class C with three different tire models viz., FTire, Pac2002 (With belt dynamics), and UA-Tire at a speed of 50 km/h . The FFT of the normal forces of the front left tire is shown in the figure 5.10.

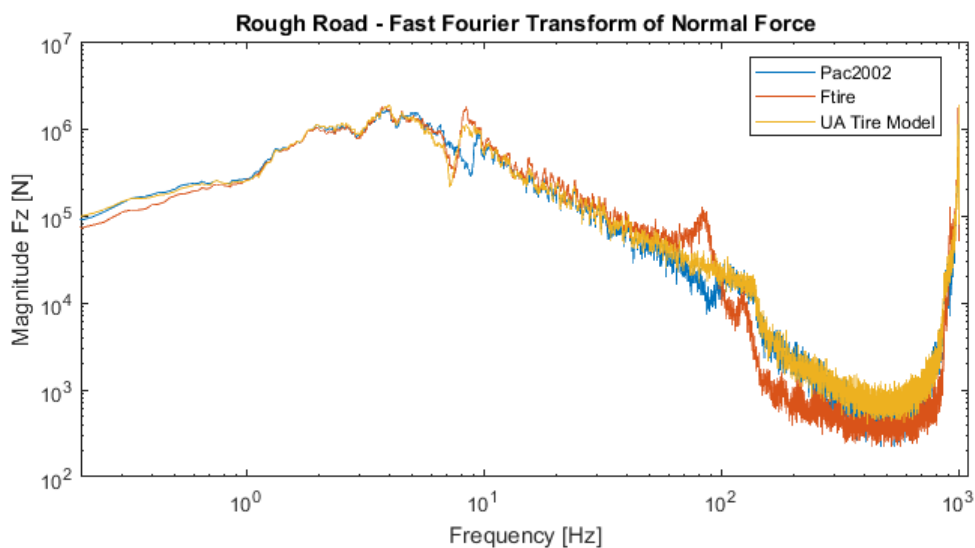


Figure 5.10: Fast Fourier Transform of the normal forces (Rough Road Impact)

Figure 5.10 shows a good correlation between the three models up to 60 Hz of frequency and beyond 60 Hz a moderate correlation can be observed with Pac2002 having a slightly better correlation with the Ftire compared to UA tire model. This is also reflected by the correlation analysis, where Pac2002 has a overall correlation of $r_{Pac} = 0.58$ and UA has a total correlation of $r_{UA} = 0.5$. Since the rough road has a combination of both short wave and long wave frequencies the effect of tire models on durability can be best observed by studying the stresses on the components, which can be observed in the below section.

5.2.4 Stress on the LCA - Rough Road

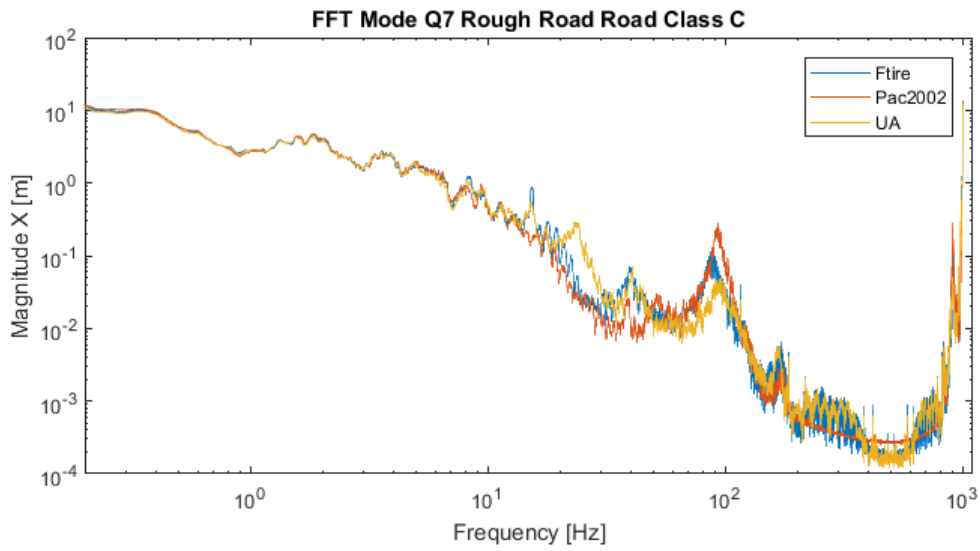


Figure 5.11: Fast Fourier Transform for Mode 7

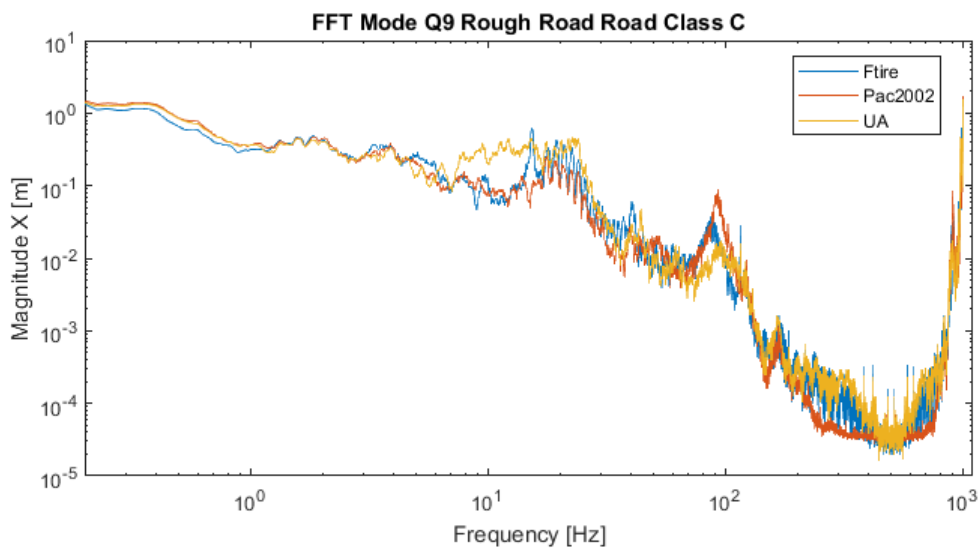


Figure 5.12: Fast Fourier Transform for Mode 9

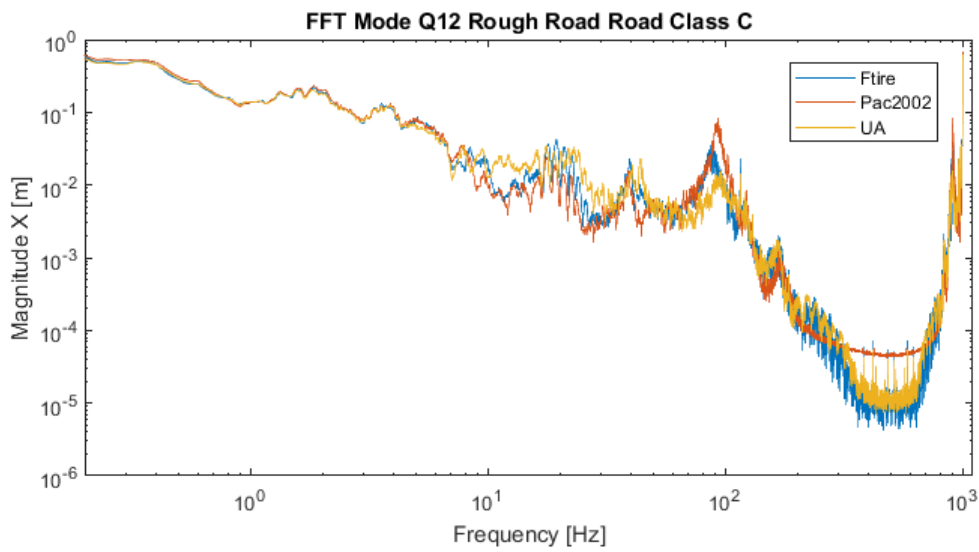
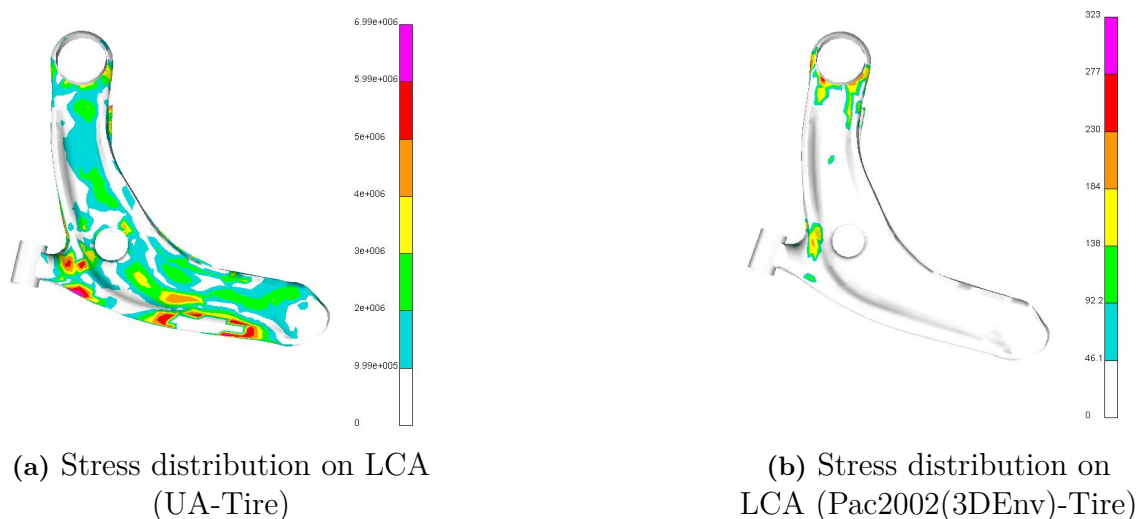


Figure 5.13: Fast Fourier Transform for Mode 12



(a) Stress distribution on LCA
(UA-Tire)

(b) Stress distribution on
LCA (Pac2002(3DEnv)-Tire)

Figure 5.14: Stress distribution on the LCA when the vehicle going over a rough road

The vehicle model was then driven over a rough road-class 3 at a speed of 50km/h with all the three tire models. The modal coordinates of the front left LCA were then obtained from ADAMS/Car and imported into FEMFAT to calculate the stress on the LCA.

It is to be noted that the simulation time for this event was chosen on the basis of trial and error, since the *run time* of the simulation increases proportionally with the *event simulation time*. Therefore, a final simulation time of 40secs was chosen so that the modal coordinates repeat thus making a cycle.

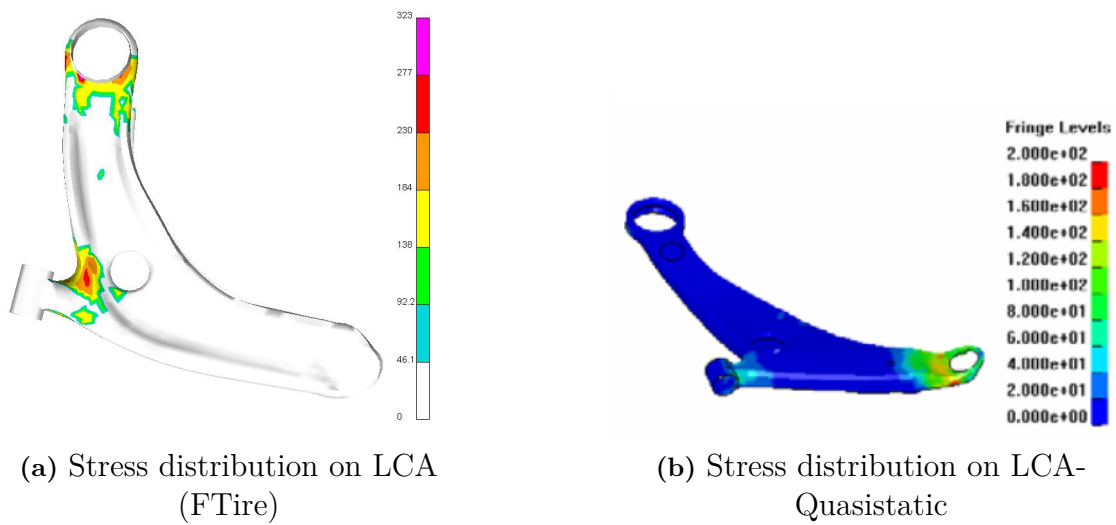


Figure 5.15: Stress distribution on the LCA - Comparison between dynamic and quasi-static simulations [5]

The figures 5.14, 5.15, and 5.16 show the FFT of the modal coordinates of modes 7, 9 and 12 respectively. From the figures it is observed that the tire model has a high influence in the modal contributions of the modal coordinates for high frequency roads. Given the same conditions, the FTire contributes more at higher frequency ranges for all the three modes. This trend is observed to continue for all the modes (318 in total) of the LCA. Therefore, these modal contributions of all the modes put together influences the stress calculation in FEMFAT.

It is seen from the figures 5.17 (a), (b) and 5.18 (a) that the stress distribution on the LCA varies significantly for each different tire model. The stress distribution on the LCA when FTire is used is found to correlate closely with the stress distribution from [5], where the load input on the LCA from proving ground tests is used for the CAE model. Whereas, the Pac2002 (3D Env) underestimates the stress distribution and the UA-Tire modes overestimates it by a considerable margin.

6

Conclusion

- The virtual durability analyses using *modal superposition* is highly feasible for concept phase vehicle development as compared to the *quasi static* method due to shorter time required for simulations and the elimination of finite element (FE) computations after the loads are obtained from MBD. Also, the effects of vibration and dynamics on the vehicle structure - which is an important factor in fatigue evaluation - could be investigated, which is not possible with the quasi static simulations.
- Fully flexible vehicle models obtained after condensation contain all the inherent properties of the FE models, at the same time, are suitable for fully dynamic simulations using MBD. But, the MBD simulation of the *complete* flexible model takes a lot of time, more so, when high fidelity tire models such as FTire and RMOD-K are used. Therefore, judicious selection of component flexibility is recommended. The component under study could be made flexible whereas other components could be made rigid to save simulation time. Also, the ratio of the *time taken* to the *results obtained*, which should ideally be less than 1, for the MBD simulations of complete flexible model and subsequently the fatigue evaluation far outweigh that of the equivalent simulation through the *quasi static* method.
- The total number of modes of the BiW reduces as the masses and windshields are added. This is because adding the windshields increases the rigidity of the structure, preventing it taking up certain mode shapes. Additionally, as the masses are added, the natural frequency of a given mode number reduces. The natural frequencies of the *global modes* obtained from simulation have been compared with the experimental natural frequencies of a similar class of vehicle obtained from the literature survey. They are found to be comparable.
- The road models developed using *OpenCRG* have been validated using the ISO standards and test data obtained from literature survey. These road models are highly accurate representation of the physical roads. The damage index for a vehicle component obtained through physical testing could be used to reproduce the road on which the vehicle was tested virtually.
- Durability studies are highly complex phenomenon involving various multi-axial loads, vibrations and dynamic effects. Therefore, the selection of suitable tire models that capture the *high frequency* vibrations and *transient dynamic*

effects is very important. Out of the three tire models compared in this thesis, *FTire* is found to be highly suitable for all kinds of road conditions. *MF-Pacejka 2002 (3D enveloping)* compares well very with *FTire* for the roads such as curb and pothole and could be used as a substitute to *FTire* for these type of roads. But, when it comes to high frequency roads such as belgian block and rough road, it is found be to lacking. The *UA-Tire* model gets the third place for all type of roads.

- It is found that the stress distribution on the LCA when *FTire* is used correlates very well with the results obtained from the quasi static simulations. Whereas, the *UA-Tire* model overestimates the stress and the *Pac2002 (3D Env)* underestimates it. As mentioned before, the quasi-static simulations do not take into account the effects of vibration, which would explain the minor discrepancies seen in the stress distribution.

7

Future Work

- Only straight line maneuvers have been considered in this work. Maneuvers on curved roads that induce lateral forces on the LCA have not been considered. Curved roads could easily be generated using the created road models and more complicated maneuvers should be performed.
- The windshields and masses of the vehicle parts should be included in the ADAMS/Car model. The influence of these masses on dynamic stress calculation were not studied in the current work due to time constraints.
- The suspension compliances such as bushes, bump stops and rebound stops and force elements such as springs and dampers must be validated by test data.
- Also, the maneuvers performed in this work have been limited to constant velocity maneuvers. Different maneuvers such as sudden acceleration and braking, braking-in-pothole, reverse curb impact etc, at different speeds should be considered and a categorization of the maneuvers causing the highest stress on the part being investigated could be performed.
- One of the bottlenecks encountered in this thesis was the time taken for the dynamic simulation of the fully flexible model. The same problem is encountered in this publication [40]. Therefore, the vehicle model should be optimized for the best requisite vehicle and simulation parameters- thereby finalizing the vehicle design- before durability simulation.
- The tire model should be validated using appropriate test data for different maneuvers - lateral as well as longitudinal.
- In this work, the fatigue life of the component was not calculated. The fatigue life of the component could be investigated by determining the number of cycles of repeating load that leads to failure.
- Sensitivity analysis of vehicle parameters on stress distribution could be investigated.
- Due to limitations in time only three roads viz., curb, pothole and rough road (class 3) were selected for simulation out of all the developed roads. The vehicle could be simulated in other developed roads such as cobblestone, washboard

7. Future Work

and different classes of rough roads.

Bibliography

- [1] Rolf Erichs *Saab Scania Story*. 1988
- [2] *Transformation 202020 Volvo*. URL:<http://m.efqm.org/25Volvo.pdf> EFQM.
- [3] Indranil Bhattacharyya, Siddharth Unadkat and Dharmendrasinh Matieda *A Durability Analysis Case Study of SUV and MUV Using Measured Proving Ground Road Profiles*. Mahindra and Mahindra Ltd 2010
- [4] Jordi Arbiol, José Antonio Muñoz, Xavierl Armengo and Enric Aramburu *Full Vehicle Durability Analysis by Means of the IDIADA Virtual Proving Ground*. Applus, IDIADA, Tarragona, Spain 2013
- [5] S.-H. Lin, C. G. Cheng and C. Y. Liao, Y.-F. Shan *CAE Analyses for Suspension System and Full Vehicle under Durability Road Load Conditions*. China Motor Corporation, Hua-chuang Automobile Information Technical Center Co.Ltd 2007
- [6] Sushanth Shandliya Dattakumar, Vivek Ganeshan *Converting dynamic impact events to equivalent static loads in vehicle chassis*. CHALMERS UNIVERSITY OF TECHNOLOGY 2017
- [7] Anders Wirje and Kristian Carlsson *Modeling and Simulation of Peak Load Events Using Adams - Driving Over a Curb and Skid Against a Curb*. Volvo Car Corporation 2011
- [8] John C. Dixon *The Shock Absorber Handbook-Second Edition*. Chapter 7: Damper Characteristics, 259-265 John Wiley and Sons Ltd, The Atrium, Southern Gate, Chichester, West Sussex PO19 8SQ, England 2007
- [9] H. Riener, D. Peiskammer, W. Witteveen - Engineering Center Steyr, Austria *A. Lion Modal Durability Analysis of a Passenger Cars Front Supporting Frame due to Full Vehicle Simulation Loads*. Volkswagen AG Wolfsburg, Germany 2001
- [10] Dr. P. Fischer, W. Witteveen, M Schabasser *Integrated MBS-FE Durability analysis of Truck Frame and Component by Modal Stresses*. Engineering Center Steyr, Technical University, Vienna 2000
- [11] Unknown Author *Theory of Flexible Bodies*, MSC Adams 2014 Online Help, 2014.
- [12] Scott Gordon *The Craig-Brampton Method*, FEMCI Presentation, 1999.
- [13] Anton Flink *Quantification and Implementation of Structural Damping in MBS Flexible Bodies*. Master Thesis in the Field of Mechanical Engineering Lund University Lund, Sweden 2015
- [14] Ying Yang, Guangyao Zhao, Dongbo Ma and Xiaobin Xu *Mode calculation and testing of a car body in white*. School of Mechanical Engineering and Automa-

- tion, Northeastern University, Shenyang, 110819, China Shenyang Aviation Vocational Technical College, Shenyang, 110043, China 2010
- [15] A. Lutz , J. Rauh and W. Reinalter *Developments in vehicle dynamics and the tire model performance test*. Vehicle System Dynamics, 45:S1, 7-19, DOI: 10.1080/00423110801925393 2008
- [16] Various *OpenCRG user manual*. VIRES Simulationstechnologie GmbH 2015.
- [17] Kim Bladh *Virtual full vehicle durability testing of a coach*. Master of Science Thesis MMK 2012:17 MKN 055 KTH Industrial Engineering and Management Stockholm, Sweden 2012
- [18] ISO 8608:2016(E) *Mechanical vibration - Road surface profiles - Reporting of measured data*. The data and plots from ISO 8608:2016 are reproduced in this report with the permission from SIS Förlag AB, www.sis.se, Tel: 08 55552310
- [19] Piet M.T. Broersen *Automatic Autocorrelation and Spectral Analysis*. Springer
- [20] Mathworks *Power Spectral Density Estimates Using FFT*.
URL:<https://se.mathworks.com/help/signal/ug/power-spectral-density-estimates-using-fft.html>
- [21] Klas Bogsjö , Krzysztof Podgórski, Igor Rychlik (2011) *Models for road surface roughness*. Vehicle System Dynamics, 50:5, 725-747, DOI:10.1080/00423114.2011.637566
- [22] Peter M *Road waviness and the dynamic tyre force*. Institute of Materials and Machine Mechanics, Slovak Academy of Sciences
- [23] Tomasz J. Kozubowski, Krzysztof Podgórski, Igor Rychlik (2013) *Multivariate generalized Laplace distribution and related random fields*. Journal of Multivariate Analysis, Vol. 113
- [24] Reza.N.Jezar *Chapter 12, Vehicle Vibrations*. Vehicle Dynamics, Theory and Applications, 3rd Edition ISBN 978-3-319-53441-1 2017.
- [25] Bernd Heissing, Metin Ersoy *Chapter 4, Axles and Suspensions*. Chassis Handbook, Fundamentals, Driving Dynamics, Components, Mechatronics, Perspectives 1st Edition ISBN 978-3-8348-0994-0 2011.
- [26] Giancarlo Genta, Lorenzo Morello *Chapter 3, Suspensions*. The Automotive Chassis, Volume 1: Component 1st Edition e-ISBN: 978-1-4020-8676-2 2009.
- [27] Geroge Rill *Chapter 6, Force Elements*. Road Vehicle Dynamics, Fundamentals and Modelling. e-ISBN: 978-1-4398-9744-7 2012.
- [28] *Introduction*. FEMFAT 5.2 user manual
- [29] Fatemi, A., Socie, D. F. 11(3), 149-165. A Critical Plane Approach to Multiaxial Fatigue Damage Including Out-Of-Phase Loading. Fatigue and Fracture of Engineering Materials and Structures. 1988
- [30] Johan Karlsson, Krzysztof Podgórski, Igor Rychlik (2015) *The Laplace multi-axial response model for fatigue analysis*. International Journal of Fatigue 85 (2016) 11-17
- [31] C. E. Rasmussen, C. K. I. Williams (2006) *Gaussian Processes for Machine Learning*. Massachusetts Institute of Technology. www.GaussianProcess.org/gpml. Pg 84-85
- [32] Simo Särkkä (2013) *State Space Representation of Gaussian Processes*. Aalto University, Espoo, Finland. Pg 22-23
- [33] Cosin scientific software *FTire - Modelization and Parameter Specification*.

- [34] Michael Gipser (2015) *ADAMS/FTire -A Tire Model for Ride and Durability Simulations*. Hochschule Esslingen
- [35] MSC Adams (2017) *Adams tire help*.
- [36] Hans B. Pacejka *Tire and Vehicle Dynamics*. Delft University of Technology
- [37] A. J. C. Schmeitz , I. J. M. Besselink and S. T. H. Jansen (2007) *TNO MFSWIFT*. *Vehicle System Dynamics*, 45:S1, 121-137, DOI: 10.1080/00423110701725208
- [38] Gim, Gwanghun (1988) *Vehicle dynamic simulation with a comprehensive model for pneumatic tires*. The University of Arisona
- [39] Kendall, M.G. (1979) *The Advanced Theory of Statistics*. 4th Ed., Macmillan
- [40] Sebastian Brandes, Klaus-Dieter Hilf, Riccardo Möller and Tobias Melz (Daimler AG and Fraunhofer Institute LBF) *Durability Simulation with Chassis Control Systems: Model Depth for a Handling Maneuver*. *Vehicle System Dynamics*, 45:S1, 7-19, DOI: 10.4271/2016-01-9111 2016

A

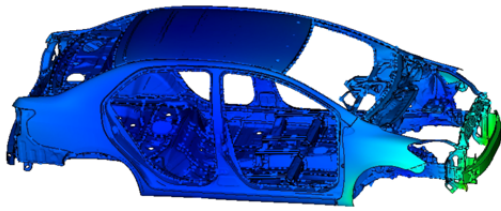
Appendix 1

A.1 Body-in-White global mode shapes

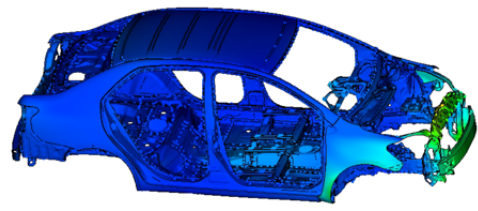
This section the global mode shapes of the BiW with and without windshields are depicted. The mode shapes are appropriately scaled to make the deformations clearer. The color code gives the deformation - *red* depicting larger deformation and *blue* smaller.

Considerable differences could be observed between the mode shapes with and without the windshields. Addition of windshields makes the structure a slightly more rigid. All the modes show some level of change in the magnitude of deformation.

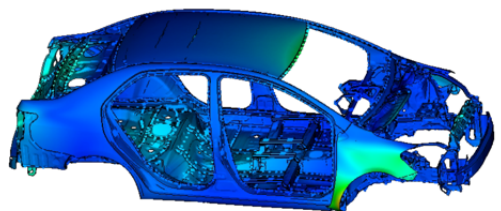
A.1.1 Without Windshields



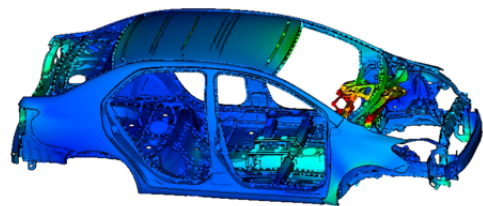
Mode 1



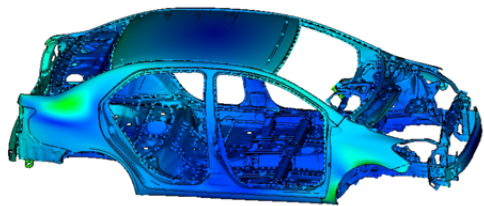
Mode 2



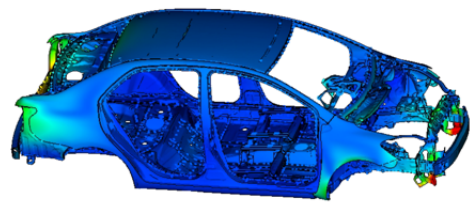
Mode 3



Mode 4



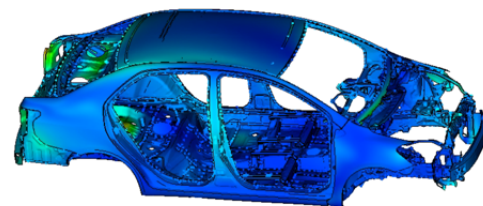
Mode 5



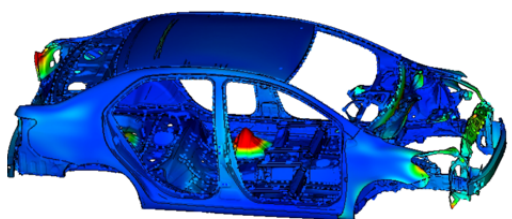
Mode 6



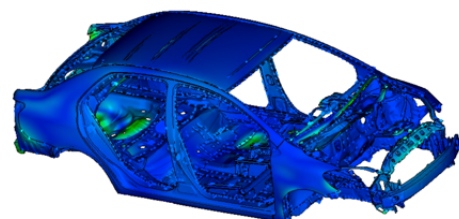
Mode 7



Mode 8



Mode 9

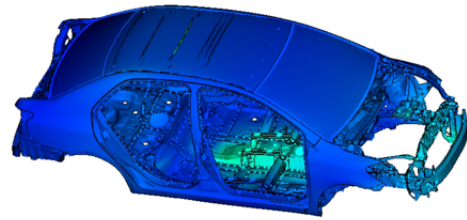


Mode 10

A.1.2 With Windshields



Mode 1



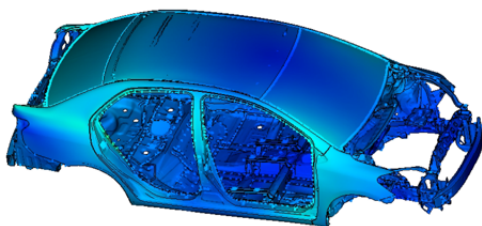
Mode 2



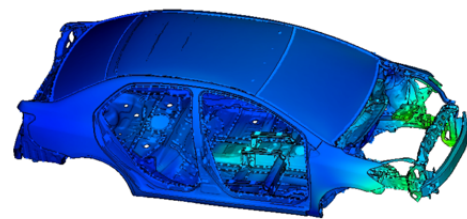
Mode 3



Mode 4



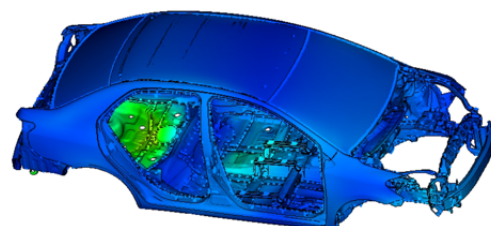
Mode 5



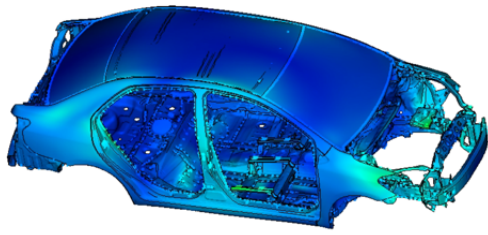
Mode 6



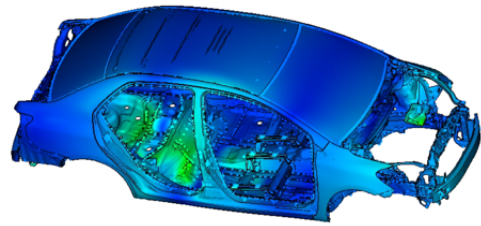
Mode 7



Mode 8



Mode 9



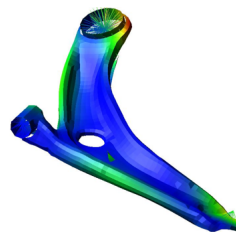
Mode 10

A.2 LCA mode shapes

The first seven modes shapes of the LCA excluding the modes 1-6 (which are the rigid body modes) are shown below.



Mode 7



Mode 8



Mode 9



Mode 10



Mode 11



Mode 12

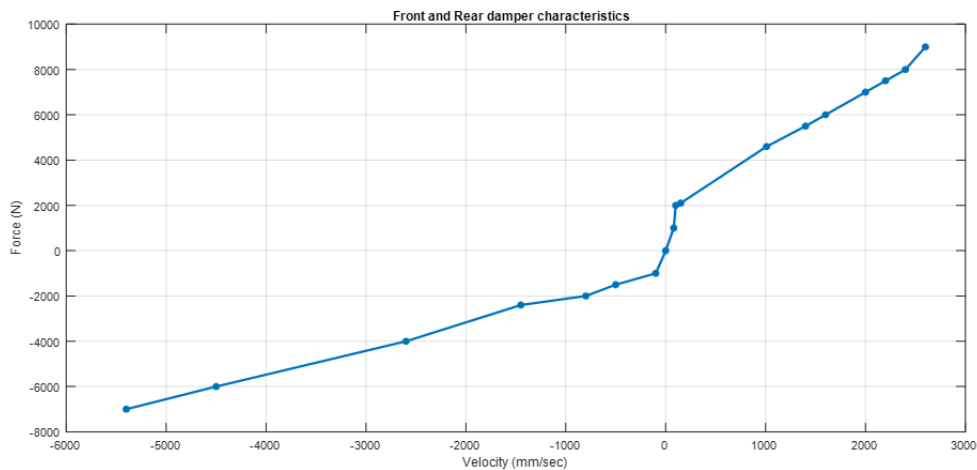


Mode 13



Mode 14

A.3 Damper Characteristics



A.4 Step size influence on normal tire forces - MF-Pacejka 2002 (3D Enveloping)

